Stem Cell Reports
Article

ISSCR

OPEN ACCESS

Cpmer: A new conserved eEF1A2-binding partner that regulates *Eomes* translation and cardiomyocyte differentiation

Yao Lyu,[1] Wenwen Jia,[1] Yukang Wu,[1] Xin Zhao,[1] Yuchen Xia,[1] Xudong Guo,[1,2,*] and Jiuhong Kang[1,*]

[1]Clinical and Translational Research Center of Shanghai First Maternity and Infant Hospital, Shanghai Key Laboratory of Maternal Fetal Medicine, Shanghai Key Laboratory of Signaling and Disease Research, Frontier Science Center for Stem Cell Research, National Stem Cell Translational Resource Center, School of Life Sciences and Technology, Tongji University, Shanghai 200092, China

[2]Institute for Advanced Study, Tongji University, Shanghai 200092, China

*Correspondence: 19504@tongji.edu.cn (X.G.), jhkang@tongji.edu.cn (J.K.)

https://doi.org/10.1016/j.stemcr.2022.03.006

SUMMARY

Previous studies have shown that eukaryotic elongation factor 1A2 (eEF1A2) serves as an essential heart-specific translation elongation element and that its mutation or knockout delays heart development and causes congenital heart disease and death among species. However, the function and regulatory mechanisms of eEF1A2 in mammalian heart development remain largely unknown. Here we identified the long noncoding RNA (lncRNA) *Cpmer* (cytoplasmic mesoderm regulator), which interacted with eEF1A2 to co-regulate differentiation of mouse and human embryonic stem cell-derived cardiomyocytes. Mechanistically, *Cpmer* specifically recognized *Eomes* mRNA by RNA-RNA pairing and facilitated binding of eEF1A2 with *Eomes* mRNA, guaranteeing *Eomes* mRNA translation and cardiomyocyte differentiation. Our data reveal a novel functionally conserved lncRNA that can specifically regulate *Eomes* translation and cardiomyocyte differentiation, which broadens our understanding of the mechanism of lncRNA involvement in the subtle translational regulation of eEF1A2 during mammalian heart development.

INTRODUCTION

Mammalian heart development is a multistep process, with multiple factors and pathways acting in concert (Murry and Keller, 2008). Proper expression of key protein-coding genes at the indicated stages is a prerequisite for heart development (Chang and Bruneau, 2012; Moore-Morris et al., 2018). Previous studies have revealed that the process of transcription of key protein-coding genes is strictly regulated during heart development. Post-transcriptional regulation of key genes, which is also essential for proteins to perform their biological functions, has not been fully investigated, especially in mammalian heart development (Simpson et al., 2020). eEF1A (consisting of eEF1A1 and eEF1A2) plays an important role in regulating translation elongation. The eEF1A1 paralog is widely expressed, but the eEF1A2 paralog is specifically expressed in the heart and brain (Liu et al., 2019). Mutation or knockout of *Eef1a2* has been shown to cause delayed heart development, congenital heart disease, and death in zebrafish, suggesting an important role of eEF1A2 in early heart development of zebrafish (Cao et al., 2017). eEF1A2 is highly conserved among species, but so far, the function and specific regulatory mechanisms of eEF1A2 in mammalian heart development remain largely unknown.

Long noncoding RNAs (lncRNAs), as tissue- and stage-specific epigenetic regulators, have attracted extensive attention for their roles in various biological processes, including heart development (Gibb et al., 2011; Wilusz et al., 2009). Previous studies have shown that Uph2 binds directly to the enhancer of *Hand2* to control its transcription and right ventricular development in mice (Anderson et al., 2016). *yylncT* promotes human embryonic stem cells (hESCs) to differentiate into mesoderm by inhibiting DNMT3B and methylation at the *T* gene promoter (Frank et al., 2019). Recent studies have also found that a cytoplasmically distributed lncRNA, *Arin*, regulates translation of *Igf2bp2* mRNA, affecting cardiomyocyte (CM) survival (Hosen et al., 2018). However, it is still necessary to investigate how lncRNAs function in translational regulation of mRNAs. Whether the heart-expressed translation elongation factor eEF1A2 acts together with specific lncRNAs and precisely regulates translation of key genes in CM differentiation has not been reported.

Eomesodermin (*Eomes*) is an important T-box transcription factor that is expressed in the primitive streak (embryonic day 6.5 [E6.5]–E7.5) of mammalian development and serves as a marker of mesoderm formation (Tosic et al., 2019). Deletion or insufficient expression of *Eomes* causes defects in mesoderm formation and heart development, eventually resulting in death. EOMES activates transcription of *Mesp1*, a key step in promoting specification of cardiac mesoderm and cardiac lineage commitment (Costello et al., 2011). Previous studies have found that Wnt (wingless/integrated) signaling can directly activate *Eomes* transcription to promote mesendodermal differentiation, and *Eomes* can also be regulated by Nodal/Smad signaling to coactivate downstream cardiac mesoderm genes (Costello et al., 2011; Teo et al., 2011; Tosic et al., 2019). lncRNAs also regulate CM differentiation in concert with EOMES.

This is an open access article under the CC BY-NC-ND license (http://creativecommons.org/licenses/by-nc-nd/4.0/).

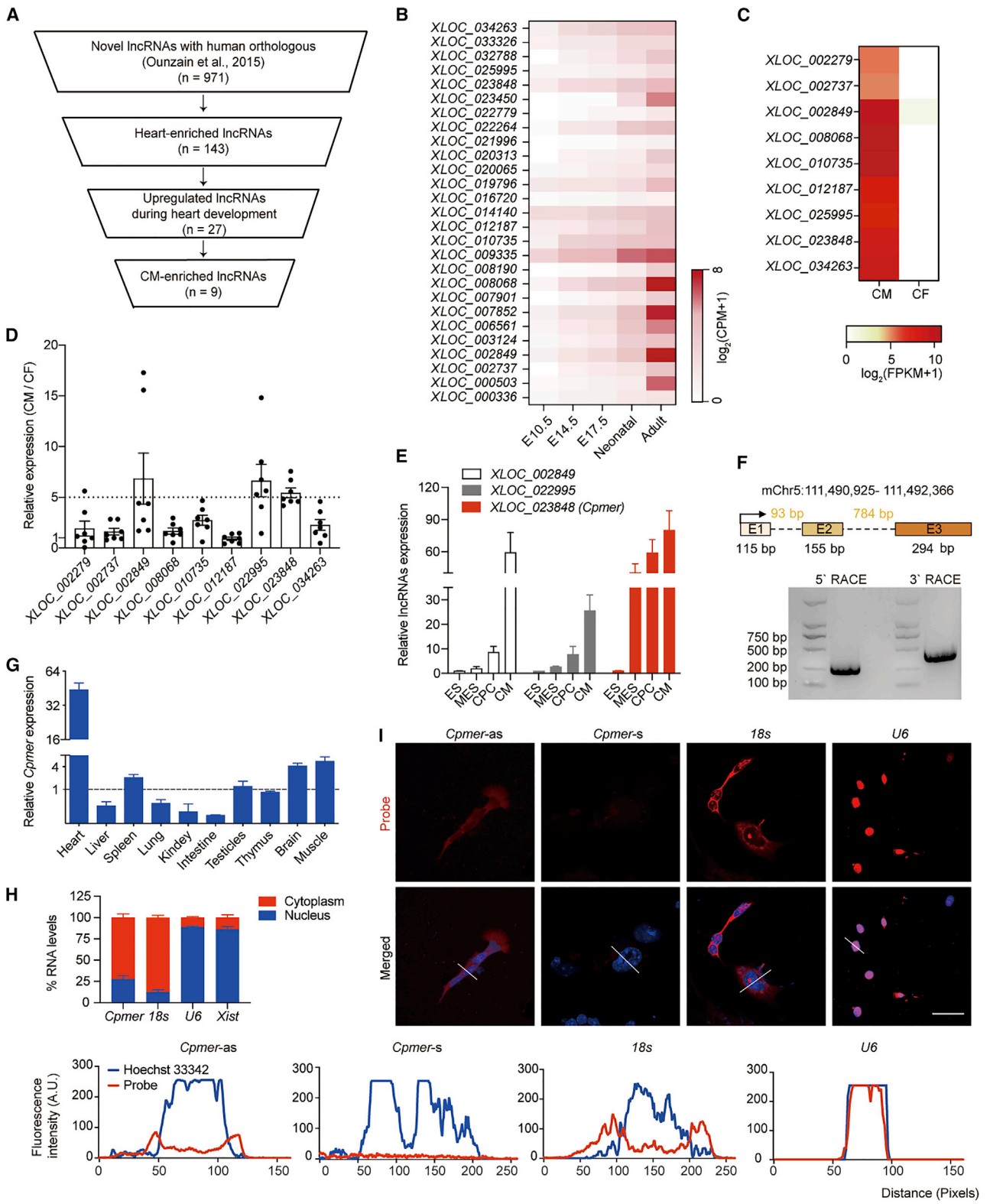

(legend on next page)

Meteor, transcribed from the enhancer region of the *Eomes* gene, regulates transcription of *Eomes* in CM differentiation (Alexanian et al., 2017). *Linc1405* (large intergenic non-coding RNA 1405) binds with EOMES and guides specific activation of EOMES at the enhancer region of the *Mesp1* gene (Guo et al., 2018). However, the specific mechanism that regulates mRNA translation of *Eomes* has not been reported.

In this study, we identified a new lncRNA (cytoplasmic mesoderm regulator [*Cpmer*]) that could interact with the translation elongation factor eEF1A2 and specifically recognize *Eomes* mRNA sequences, contributing to proper translation of *Eomes* mRNA and CM differentiation. We observed that the human ortholog *CPMER* had consistent effects on eEF1A2 binding and translational regulation of human *EOMES* mRNA.

RESULTS

Cpmer is a potentially important cytoplasmic lncRNA in CM differentiation

To investigate the function of unknown lncRNAs in regulating CM differentiation, we analyzed RNA sequencing (RNA-seq) data that had been used to identify a set of novel lncRNAs in the murine heart and focused on novel transcripts with putative human orthologs; we narrowed it down to 971 transcripts (Ounzain et al., 2015). Then we analyzed differentially expressed transcripts on the indicated days (E10.5, E14.5, E17.5, neonatal, and adult) of mouse heart development (GSE158202) and identified 143 transcripts specifically enriched in the heart, 27 of which were positively correlated with the heart development process (Figures 1A and 1B; Table S1). 9 of the candidate lncRNAs were found to be enriched in CMs (Mullin et al., 2017; Figure 1C), and qRT-PCR results confirmed that 3 (*XLOC_002489*, *XLOC_022995*, and *XLOC_023848*) of these 9 lncRNAs were expressed at 5-fold higher levels in CMs than in cardiac fibroblasts (CFs) (Figure 1D). The expression levels of these 3 lncRNAs were quantified during CM differentiation, and we found that expression of *XLOC_023848*, hereafter called *Cpmer* (GenBank: OL365371), was significantly upregulated at the mesoderm stage, suggesting that *Cpmer* might be important in regulating CM differentiation (Figure 1E). *Cpmer* was located at mm10 chromosome 5 (111,490,925–111,492,366) and consisted of three exons near the protein-coding gene *Mn1*. Rapid amplification of cDNA ends (RACE) was employed to amplify the full-length *Cpmer* transcript (Figure 1F). *Cpmer* was specifically expressed in the heart of mice compared with other fetal tissue (Figure 1G). Coding potential analysis of *Cpmer* indicated that it had low coding potential, similar to *Xist* (Figure S1A). We also analyzed the ribosome profiling sequencing (Ribo-seq) data of mesoderm cells (GSE86467; Fujii et al., 2017) and found that there were no mapping reads at the genomic location of *Cpmer*, suggesting that the ribosome was not occupied on *Cpmer*. These results confirmed that *Cpmer* did not have the potential for protein coding (Figure S1B). Nuclear/cytoplasmic fractionation analysis and RNA fluorescence *in situ* hybridization (FISH) confirmed the cytoplasm distribution of *Cpmer* in mesoderm cells (Figures 1H and 1I). These data suggest that *Cpmer* may play a functional role in regulating cardiac differentiation in the cytoplasm.

Cpmer is critically required for proper CM differentiation

Next, to explore the role of *Cpmer* in CM differentiation, we constructed *Cpmer* knockout (KO-*Cpmer*) mouse embryonic stem cell (mESC) 46C cell line using CRISPR-Cas9

Figure 1. *Cpmer* is a potentially important cytoplasmic lncRNA in CM differentiation

(A) Strategy for selecting novel lncRNAs related to heart development.

(B) The expression pattern of selected lncRNAs on the indicated days of mouse development. CPM, counts per million.

(C) Heatmap of the lncRNAs significantly enriched in CMs compared with cardiac fibroblasts (CFs). FPKM, fragments per kilobase of exon model per million mapped fragments.

(D) Validation of lncRNA expression in CMs versus CFs. Data shown are mean ± SEM, n = 7 mice.

(E) The expression pattern of candidate lncRNAs during CM differentiation. MES, mesoderm cells. Data shown are mean ± SEM, n = 3 independent experiments.

(F) Detection of 5′ and 3′ termini of *Cpmer* by RACE.

(G) Histograms showing the relative expression levels of Cpmer in neonatal mouse tissues. The mean of expression levels of *Cpmer* in the listed tissues was taken as 1 (dashed line). Data represent mean ± SEM, n = 3 mice.

(H) qRT-PCR analysis of the RNAs (*Cpmer*, *18s*, *U6*, and *Xist*) derived from the cytosolic or nuclear fractions of MESs. Data shown are mean ± SEM, n = 3 independent experiments.

(I) RNA FISH assay showing the representative images of the *Cpmer*-antisense (*Cpmer*-as) probe targeting *Cpmer* in MESs (top). The *Cpmer*-sense (*Cpmer*-s) probe served as a negative control. *U6*, positive control for nuclear RNA; *18s*, positive control for cytoplasmic RNA. Nuclei were stained with Hoechst 33342 (blue). Scale bar, 20 μm. The variation patterns of the RNA probe and nuclear signals were analyzed (bottom).

See also Figure S1 and Table S1.

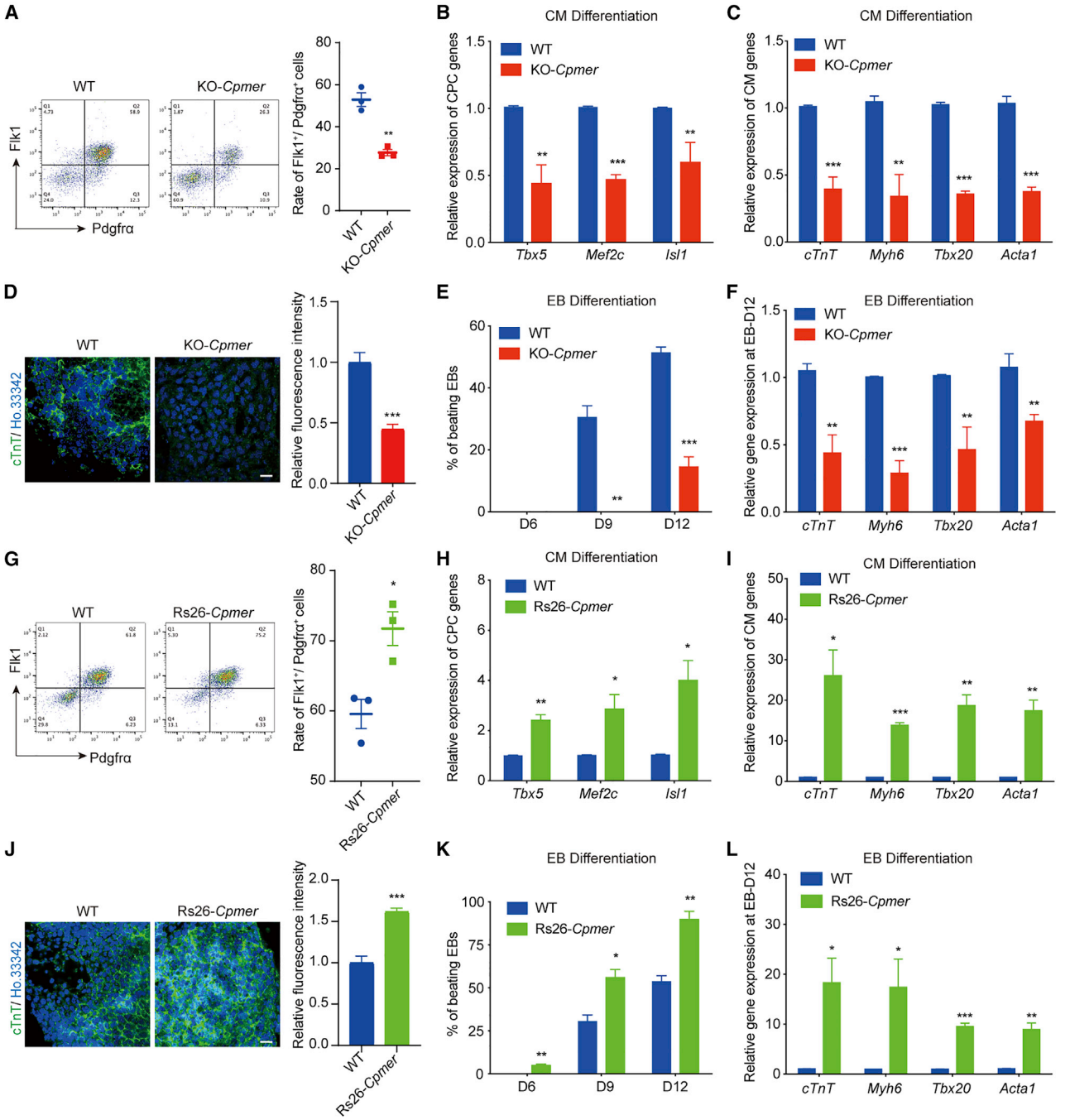

Figure 2. *Cpmer* is critically required for proper CM differentiation

(A) FACS analysis and statistics for the percentage of Flk1$^+$Pdgfrα^+ cells. Data shown are the mean ± SEM, n = 3 independent experiments.

(B and C) qRT-PCR analysis of CPC (B) and CM (C) marker genes. Data shown are the mean ± SEM, n = 3 independent experiments.

(D) cTnT immunostaining (green) at the CM stage (left) and statistics for relative fluorescence intensity (right). Scale bar, 20 μm. Data shown are the mean ± SEM, n = 6 fields from 3 independent experiments.

(E) Percentage of spontaneously contracting EBs determined on days 6, 9, and 12 of EB differentiation. Data shown are the mean ± SEM, n = 3 independent experiments.

(F) qRT-PCR analysis of CM marker genes on day 12 of EB differentiation (EB-day 12). Data shown are the mean ± SEM, n = 3 independent experiments.

(G) FACS analysis and statistics of the percentage of Flk1$^+$Pdgfrα^+ cells. Data shown are the mean ± SEM, n = 3 independent experiments.

(legend continued on next page)

technology (Figure S2A). Our data showed that KO of *Cpmer* did not affect the expression level of pluripotency genes or of its neighbor gene *Mn1* (Figures S2B–S2D) but significantly reduced the percentage of Flk1$^+$/Pdgfrα^+ cells that appeared at the mesoderm stage (Figure 2A). Moreover, cardiac progenitor cell (CPC) marker genes (*Tbx5*, *Gata4*, and *Mef2c*) and CM marker genes (*cTnT*, *Myh6*, *Tbx20*, and *Acta1*) exhibited lower expression levels in KO-*Cpmer* cells (Figures 2B and 2C). KO of *Cpmer* resulted in a lower proportion of cTnT$^+$ CMs than wild-type (WT) cells (Figure 2D). Similarly, KO of *Cpmer* led to a delay in spontaneous contraction compared with WT cells (spontaneous contraction appeared on day 8, and the contraction rate was about 30% on day 9 and 60%–70% on day 12) (Figure 2E). Expression of cardiac genes was significantly decreased in KO-*Cpmer* cells on day 12 of embryoid body (EB) differentiation (Figure 2F). KO of *Cpmer* did not affect the neuroectoderm and definitive endoderm differentiation but resulted in upregulated expression of marker genes of CFs and endothelial cells and decreased expression of smooth-muscle-related genes (Figures S2E and S2F).

We then inserted the full-length *Cpmer* sequence into the ROSA26 locus (used for constitutive gene expression) to increase *Cpmer* expression (Rs26-*Cpmer*) (Figure S2G). Overexpression of *Cpmer* had no effect on expression of pluripotency genes and the neighbor gene *Mn1* (Figures S2H–S2J). Fluorescence-activated cell sorting (FACS) assays showed that *Cpmer* overexpression significantly increased the percentage of Flk1$^+$/Pdgfrα^+ mesoderm cells (Figure 2G), along with increased expression of CPC and CM marker genes (Figures 2H and 2I) and ratio of cTnT$^+$ cells in Rs26-*Cpmer* cells (Figure 2J). Spontaneously contracted EBs appeared earlier in *Cpmer*-overexpressing cells, on day 6, along with an increased beating ratio and cardiac marker expression (Figures 2K and 2L). In contrast, the expression levels of CF and endothelial cell markers were attenuated in Rs26-*Cpmer* cells compared with WT cells (Figure S2K). These results indicate that *Cpmer* plays a critical role during proper CM differentiation.

eEF1A2 is a *Cpmer*-binding protein and similarly regulates CM differentiation

Because cytoplasmic lncRNAs usually interact with RNA-binding proteins to execute their cellular functions, we performed an RNA pull-down assay followed by mass spectrometry analysis to identify the interactome of *Cpmer* (Figure 3A; Table S2). Among the potential interaction proteins of *Cpmer*, eEF1A2, usually expressed in terminally differentiated cells (i.e., CMs and nerve cells), exhibited a remarkable interaction intensity with *Cpmer* (Figure 3A). Binding of *Cpmer* and FLAG-eEF1A2 was confirmed by exogenous RNA immunoprecipitation (RIP) experiments (Figure 3B). An endogenous RNA pull-down assay mediated by MS2bp-YFP (yellow fluorescent protein) also confirmed that *Cpmer* interacted with eEF1A protein in mesoderm cells (unable to distinguish eEF1A2 from eEF1A1 with an anti-eEF1A antibody) (Figure 3C). Similar to *Cpmer* expression, *Eef1a2* expression was significantly increased during CM differentiation and was specifically detected in the heart of fetal mice (Figures 3D and 3E).

We constructed *Eef1a2* knockdown mESC lines by short hairpin RNA (shRNA) viruses, which were confirmed at the mRNA and protein levels (Figure 3F). Our findings showed that *Eef1a2* knockdown led to a significant decrease in the percentage of Flk1$^+$/Pdgfrα^+ cells and the mRNA expression levels of CPC and CM marker genes compared with control group (sh-Ctrl) (Figures 3G–3I). Immunofluorescence analysis confirmed a significant reduction in cTnT$^+$ cells after *Eef1a2* knockdown (Figure 3J). The results of EB differentiation confirmed that *Eef1a2* knockdown resulted in a decreased percentage of beating EBs and expression of CM marker genes (Figures 3K and 3L). These results indicate that the translation elongation factor eEF1A2 serves as a potential partner of the lncRNA *Cpmer* in CM differentiation.

Cpmer/eEF1A2 recognizes the mRNA of the mesoderm gene *Eomes* and regulates its translation

We sought to investigate the mechanism by which *Cpmer*/eEF1A2 regulates CM differentiation and analyzed the potential mRNAs (791 genes) that theoretically interacted with *Cpmer* via RNA pairing by RIblast (Table S3; Fukunaga and Hamada, 2017). 3 genes (*Eomes*, *Bmp4*, *and Lef1*) were found when overlapping with genes associated with mesoderm formation (GO_ID: 00010707) (Figure S3A). Among these genes, *Eomes* was thought to be a well-known transcription factor in the mesoderm and significantly increased at the mesoderm stage (Figure S3B). We confirmed that knockdown of *Eomes* significantly reduced the percentage of spontaneously beating EBs and decreased

(H and I) qRT-PCR analysis of CPC (H) and CM (I) marker genes. Data shown are the mean ± SEM, n = 3 independent experiments.
(J) cTnT immunostaining (green) at the CM stage (left) and statistics for relative fluorescence intensity (right). Scale bar, 20 μm. Data shown are the mean ± SEM, n = 6 fields from 3 independent experiments.
(K) Percentage of spontaneously contracting EBs of EB differentiation. Data shown are the mean ± SEM, n = 3 independent experiments.
(L) qRT-PCR analysis of CM marker genes at EB-day 12. Data shown are the mean ± SEM, n = 3 independent experiments. *p < 0.05, **p < 0.01, ***p < 0.001 (versus WT); Student's t test.
See also Figure S2.

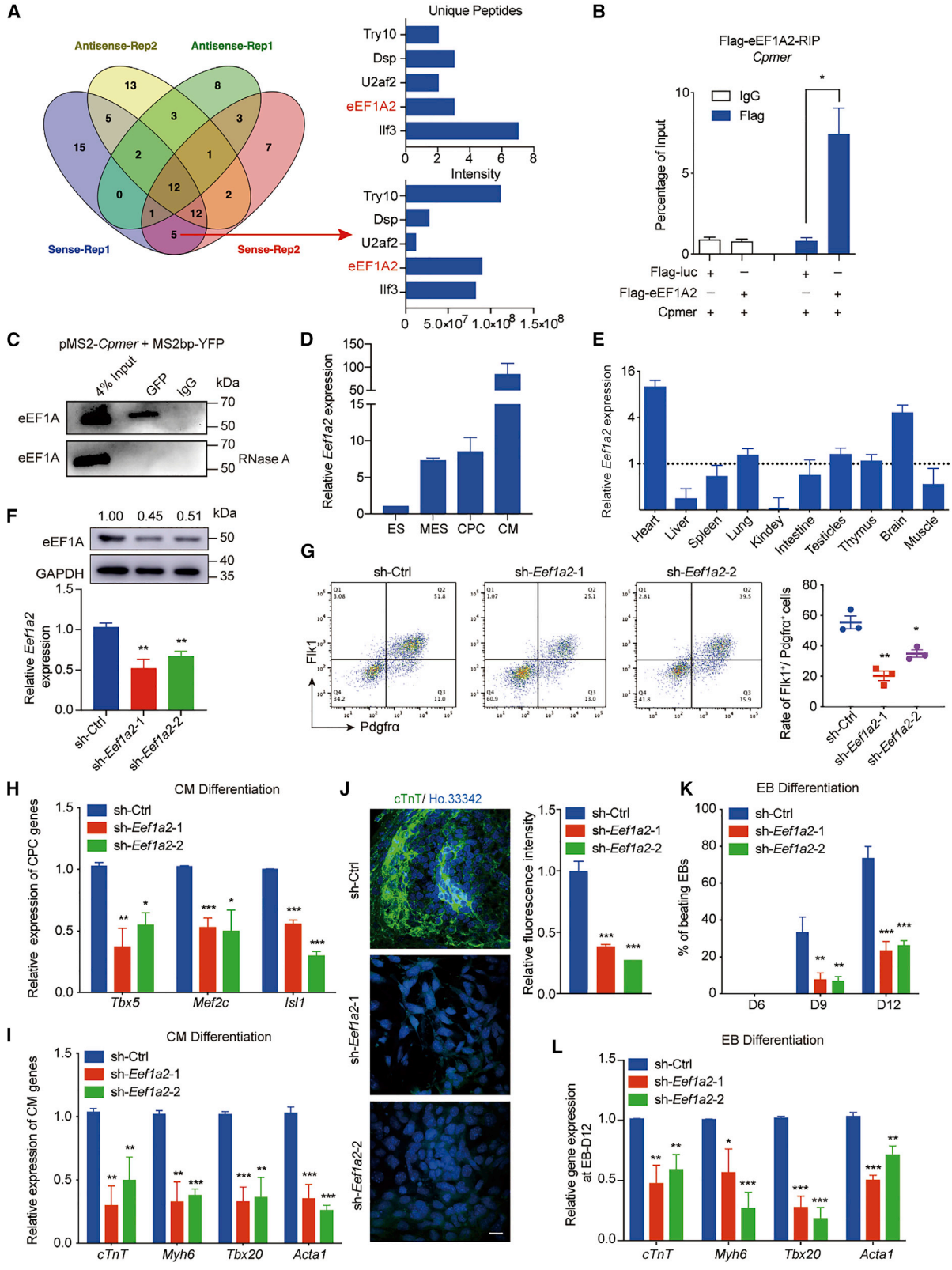

(legend on next page)

the expression levels of CM markers on day 12 of EB differentiation (Figures S3C–S3E). Bone morphogenetic protein 4 (*Bmp4*), as a secreted ligand of the transforming growth factor β (TGF-β) superfamily, mainly functions in differentiation of pluripotent stem cells (PSCs) into the mesodermal instead of the ectodermal lineage (Johansson and Wiles, 1995; Monteiro et al., 2004). *Lef1*, as a response molecule of Wnt/β-catenin signaling, has been reported to be associated with neurogenesis and T cell differentiation, whereas deletion of *Lef1* did not affect cardiogenesis (Galceran et al., 1999; Oosterwegel et al., 1993; Xing et al., 2019). Previous studies have reported that BMP4 treatment can upregulate expression of *Eomes* and *T* (another key mesoderm transcription factor), whereas deficiency of *Bmp4* resulted in significant downregulation of *Eomes* and *T* in embryos (Amita et al., 2013; Soares et al., 2005), suggesting that BMP4 might serve as the upstream regulator of the *Eomes* and *T* genes. Our findings showed that the mRNA expression levels of *Eomes* and *T* were not influenced by *Cpmer* (Figure 4A), indicating that *Bmp4* was not a target of *Cpmer*. The protein level of EOMES, but not T, was significantly decreased in KO-*Cpmer* mesoderm cells (Figures 4B and 4C). Thus, we speculated that *Cpmer* might affect the protein level of EOMES at the mesoderm stage.

Analysis of the potential interaction of *Cpmer* and *Eomes* mRNA indicated RNA pairing between the third exon of *Cpmer* and the coding sequence (CDS) region of *Eomes* (95–125 nt) (Figure 4D). To demonstrate the potential binding of *Cpmer* and the *Eomes* mRNA, we constructed *Eomes* full-length (Myc-*Eomes*-FL), Myc-*Eomes*-ΔBS (deletion of the predicted binding sequences [BSs]), and Myc-*Eomes*-ΔELS (deletion of equal-length sequences [ELSs]) overexpression vectors (Figure 4E). The exogenous RNA pull-down assay showed that the *Eomes* mRNA interacted with *Cpmer* via the predicted BS (Figure 4F). We then studied whether the interaction between *Cpmer* and the *Eomes* mRNA affected expression of the EOMES protein. When transfecting FL and deletion mutant *Eomes* into WT cells, our results showed that the protein level of exogenous *Eomes*-ΔBS was significantly lower than that of FL *Eomes* and *Eomes*-ΔELS (Figure 4G). Similarly, deficiency of *Cpmer* impaired the protein expression level of FL *Eomes* or its deletion mutants but not the mRNA level (Figure 4H). The expression level of EOMES protein remained quite low in KO-*Cpmer* cells compared with WT cells with or without transfection of FL *Eomes* (Figure S3F). We constructed GFP reporters by separately inserting the BS of *Eomes* mRNA and *Cpmer* (BS), the ELS (as a scramble sequence), and the antisense BS (anti-BS) upstream of the GFP gene and then introduced these GFP reporters into the WT and KO-*Cpmer* cell lines (Figure 4I). The fluorescence intensity of BS-GFP was significantly stronger than that of ELS-GFP or anti-BS-GFP in WT mesoderm cells, suggesting that the BS of *Eomes* mRNA with *Cpmer* facilitated GFP mRNA translation. The fluorescence intensity of all GFP reporters was extremely low in KO-*Cpmer* mesoderm cells, indicating that *Cpmer* was required for proper GFP mRNA translation (Figure 4J). Considering that the effect of *Cpmer* KO occurred at the post-transcriptional level, we then treated mesoderm cells with actinomycin D or MG132 to detect mRNA stability or protein degradation. KO of *Cpmer* did not affect the stability of *Eomes* and *T* mRNAs or degradation of EOMES or T protein (Figures S3G and S3H). These results indicated that the direct RNA-RNA pairing of *Cpmer* and *Eomes* greatly affects Eomes mRNA translation.

The RIP assay showed that eEF1A interacted with *Eomes* mRNA in WT cells but not in KO-*Cpmer* cells (Figure 4K).

Figure 3. eEF1A2 is a *Cpmer*-binding protein and similarly regulates CM differentiation

(A) MS to identify the potential *Cpmer*-binding proteins (left). The unique peptides and intensities of 5 candidate proteins are shown (right).

(B) RIP analysis for exogenous expression of *Cpmer* and FLAG-eEF1A2 in 293T cells, determined by an anti-FLAG antibody. Data shown are the mean ± SEM, n = 3 independent experiments.

(C) MS2bp-YFP RNA pull-down analysis for the co-transfected pMS2-*Cpmer* and MS2bp-YFP in MESs with or without RNase A treatment. An anti-GFP antibody was used to recognize the YFP protein.

(D) The expression pattern of *Eef1a2*. Data shown are the mean ± SEM, n = 3 independent experiments.

(E) The relative expression levels of *Eef1a2* in neonatal mouse tissues. Data shown are the mean ± SEM, n = 3 mice.

(F) Detection of mRNA and protein expression levels of *Eef1a2* at the MES stage after *Eef1a2* knockdown. Data shown are the mean ± SEM, n = 3 independent experiments.

(G) FACS analysis and statistics of the percentage of $Flk1^{+}Pdgfr\alpha^{+}$ cells. Data shown are the mean ± SEM, n = 3 independent experiments.

(H and I) qRT-PCR analysis of CPC (H) and CM (I) marker genes. Data shown are the mean ± SEM, n = 3 independent experiments.

(J) cTnT immunostaining (green) at the CM stage (left) and statistics for relative fluorescence intensity (right). Scale bar, 20 μm. Data shown are the mean ± SEM, n = 6 fields from 3 independent experiments.

(K) Percentage of spontaneously contracting EBs of EB differentiation. Data shown are the mean ± SEM, n = 3 independent experiments.

(L) qRT-PCR analysis of the CM marker genes. Data shown are the mean ± SEM, n = 3 independent experiments. *p < 0.05, **p < 0.01, ***p < 0.001 (versus sh-Ctrl); Student's t test.

See also Table S2.

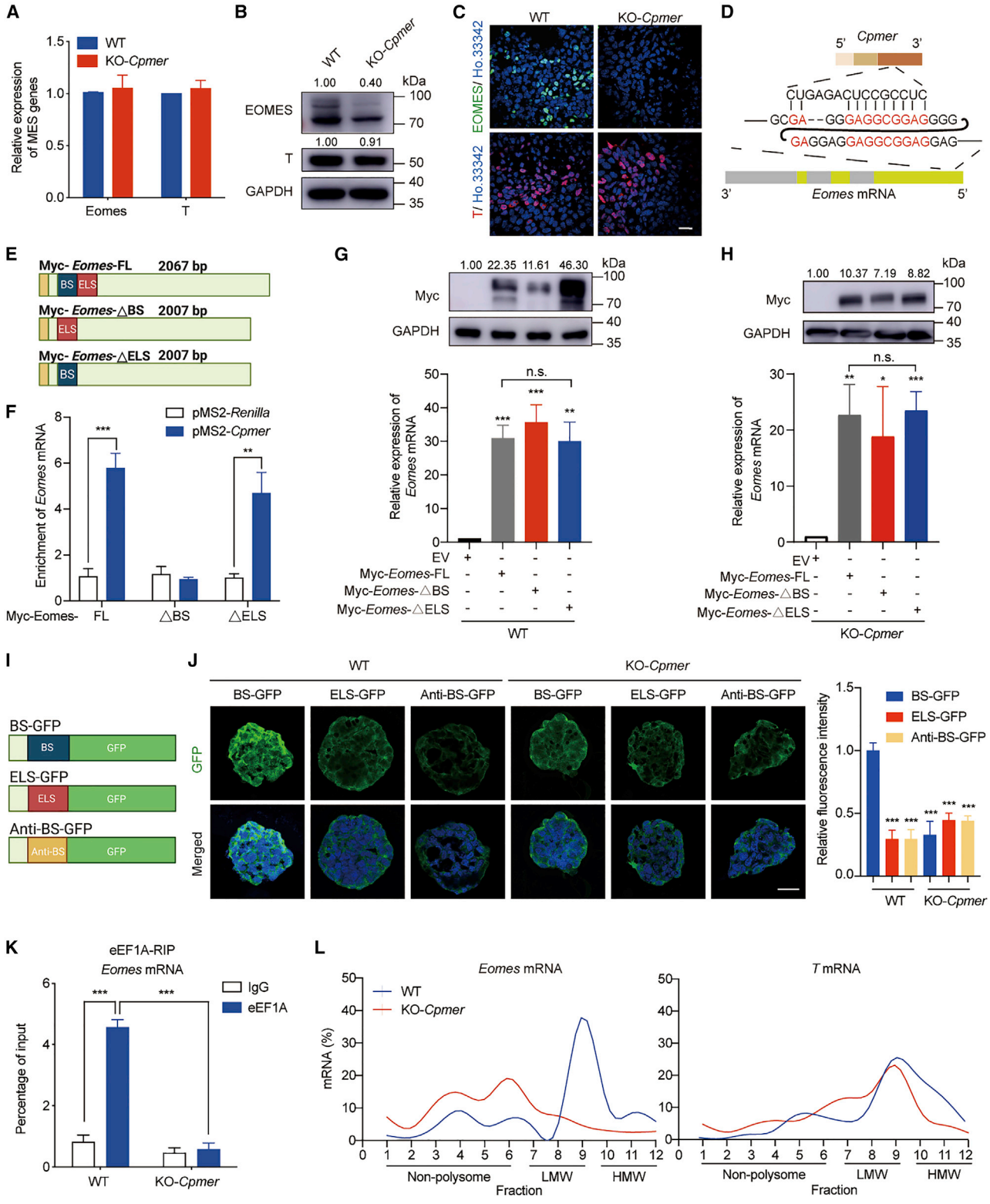

Figure 4. *Cpmer*/eEF1A2 recognizes mRNA of the mesoderm gene *Eomes* and regulates its translation

(A–C) qRT-PCR (A), western blot (B), and immunofluorescence (C) detection of the expression of representative mesodermal marker genes (*Eomes* and *T*). Data shown are the mean ± SEM, n = 3 independent experiments. Scale bar, 20 μm.

(legend continued on next page)

A previous study has shown that eEF1A2 directly interacts with the *Utrn* mRNA (Miura et al., 2010). Enrichment of eEF1A2 on *Utrn* mRNAs was not affected by *Cpmer* KO, suggesting that *Cpmer* mediated the specific binding of eEF1A2 and the *Eomes* mRNA (Figure S3I). KO of *Cpmer* did not affect expression of *Eef1a2* or other translation-related elements (*Eef1a1*, *Eif2a*, *Rpl3*, and *Rpsa*) (Figure S3J), suggesting that *Cpmer* might act as a scaffold for proper binding of eEF1A2 and the *Eomes* RNA. A polysome profile assay followed by qRT-PCR showed that loss of *Cpmer* resulted in low enrichment of the polysome fraction (fractions 7–12) on *Eomes* mRNA but not *T* (Figures 4L and S3K), suggesting specificity of *Cpmer*-mediated *Eomes* translation. Distribution of eEF1A in the polysome fractions showed no significant change in WT and KO-*Cpmer* cells, which suggested that eEF1A recruitment to ribosomal complexes was independent of *Cpmer* (Figure S3L). Consistent with the finding that eEF1A2 was mainly involved in translational regulation of genes, we concluded that *Cpmer* recruited eEF1A2 on *Eomes* mRNA by RNA-RNA recognition, regulating its translation.

E23 of *Cpmer* is responsible for *Eomes* translation and CM differentiation

We then constructed plasmids overexpressing *Cpmer* fragments (E1, E2, and E3) (Figure S4A), and only the second fragment of *Cpmer* (E2) interacted with the eEF1A2 protein (Figures S4B and S4C). Overexpression of an individual *Cpmer* fragment neither affected the mRNA levels of *Eomes* and *T* at the mesoderm stage (Figure S4D) nor rescued the protein level of EOMES (Figure S5E) or the ratio of spontaneously beating EBs (Figure S4F). We then constructed overexpression plasmids containing two exons of *Cpmer* (E12, E23, and E13) (Figure 5A) and found that only the *Cpmer* mutant E23 could recover enrichment of the eEF1A2 protein on *Eomes* mRNA (Figure 5B). Accordingly, overexpression of E23 rescued polysome enrichment and EOMES protein expression in KO-*Cpmer* cells, whereas the other two *Cpmer* mutants (E12 and E13) were not able to rescue expression of the EOMES protein (Figures 5C–5F). FACS assays also showed that the ratio of $Flk1^+$/$Pdgfr\alpha^+$ cells, the ratio of beating EBs, and CM marker expression could be rescued only by E23 overexpression (Figures 5G–5I). We also analyzed the RNA structure of *Cpmer* by RNAfold, and these results showed that FL and E23 of *Cpmer* contained unique stem-loop structures with low positional entropy (Figures S5G and S5H). Neither E1 nor E13 of *Cpmer* contained a similar structure (Figures S5I and S5J), which suggested that the stem-loop structure of *Cpmer* might be considered its protein-binding characteristic. Combined with the finding that *Cpmer* bound to the eEF1A protein and *Eomes* mRNA through the distinct RNA fragments E2 and E3, respectively, these data indicate that *Cpmer* establishes a link between the eEF1A2 protein and *Eomes* mRNA, which ensures *Eomes* translation and proper cardiac differentiation.

Because *Cpmer* levels kept rising during CM differentiation and sustained high expression in CMs, but the expression level of *Eomes* was significantly increased at the mesoderm stage and decreased rapidly after mesoderm differentiation, we were curious about the roles of *Cpmer* after mesoderm differentiation. Surprisingly, it was found that there were 33 mRNAs overlapped with potentially recognized mRNAs and genes associated with heart development (GO_ID: 0007507), including *Tbx18* and *Tbx20* (CPC transcription factors) and *cTnT* (a CM marker) (Figure S5A). We effectively knocked down *Cpmer* by shRNA virus after the mesoderm stage, and our results showed that knockdown of *Cpmer* after the mesoderm stage also resulted in lower expression levels of CM marker genes compared with the control (Figures S5B and S5C), as well as the lower proportion of $cTnT^+$ CMs (Figure S5D). Hence, we believed that *Cpmer* might target distinct mRNAs during CM differentiation and that its recognition and regulation of Eomes mRNA at the mesoderm stage was critical for proper CM differentiation.

(D) Regions of potential recognition between *Cpmer* and mouse *Eomes* mRNA.
(E) Schematic of the FL and deletion mutants of *Eomes* mRNA. BS, blue; ELS, red; Myc tag, yellow.
(F) MS2bp-YFP RNA pull-down analysis for exogenous expression of *Cpmer* with FL or deletion mutant *Eomes* mRNA in 293T cells. pMS2-*Renilla* RNA was used as a negative control. The fold enrichment relative to the immunoglobulin G (IgG) control is shown. Data shown are the mean ± SEM, n = 3 independent experiments.
(G and H) qRT-PCR and western blot analysis of *Eomes* mRNA and protein levels in WT (G) or KO-*Cpmer* (H) cells transfected with FL or deletion mutant *Eomes*. Data shown are the mean ± SEM, n = 3 independent experiments.
(I) Schematic of the GFP reporters. BS, blue; ELS, red; anti-BS, yellow.
(J) GFP signal analysis at EB-day 4 in cells transfected with distinct GFP reporters (left) and statistics for relative GFP signal intensity (right). Scale bar, 20 μm. Data shown are the mean ± SEM (n = 6 fields from 3 independent experiments).
(K) RIP analysis of the interaction of eEF1A with *Eomes* mRNA. Data shown are the mean ± SEM, n = 3 independent experiments.
(L) Percentage of *Eomes* and *T* mRNAs in the gradient total RNA, as measured by qRT-PCR in each fraction collected from the polysome profiling assay. LMW, low molecular weight; HMW, high molecular weight. *p < 0.05, **p < 0.01, ***p < 0.001; n.s., not significant; Student's t test.
See also Figures S3 and S4 and Table S3.

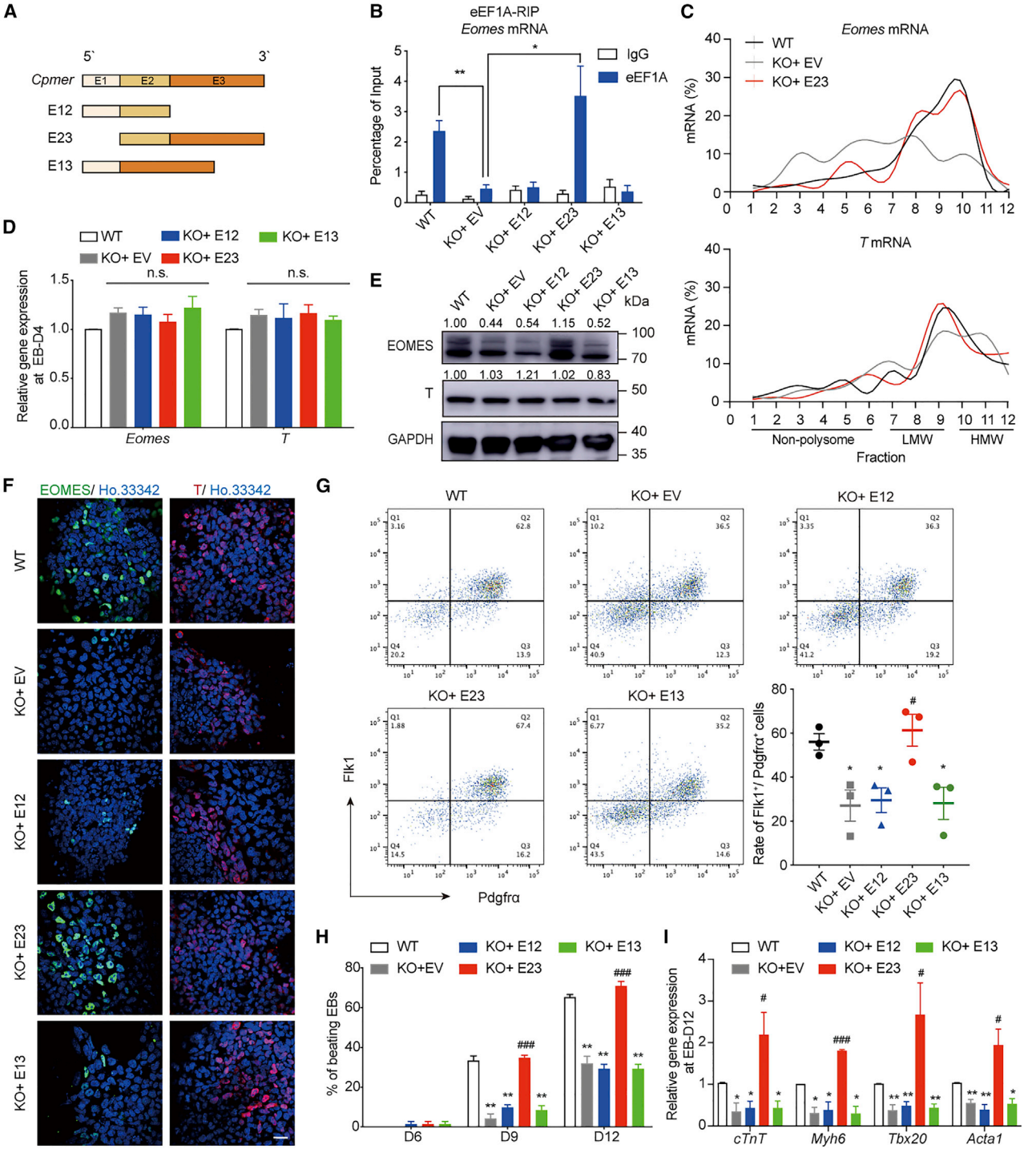

Figure 5. E23 of *Cpmer* is responsible for *Eomes* translation and CM differentiation

(A) Schematic of *Cpmer* mutants.

(B) RIP analysis of eEF1A binding with *Eomes* mRNA in KO-*Cpmer* cells transfected with *Cpmer* mutants. Data shown are the mean ± SEM, n = 3 independent experiments.

(C) Polysome profile analysis of *Eomes* and *T* mRNAs.

(D–F) qRT-PCR (D), western blot (E), and immunofluorescence (F) detection of expression of *Eomes* and *T*. Data shown are the mean ± SEM, n = 3 independent experiments. Scale bar, 20 μm.

(legend continued on next page)

CPMER/eEF1A2 conservatively functions in *EOMES* translation and human CM differentiation

CPMER (ENST00000440255.1) was identified as a putative ortholog of *Cpmer* in the human genome (hg38 chromosome 22: 27,676,559–27,714,970). We first detected the stage-specific makers of hESC-derived CM differentiation (Figure S6A) and found that expression of *CPMER* was similarly upregulated at the mesoderm stage (Figure 6A). Next, two *CPMER* knockdown cell lines were constructed, and knockdown of *CPMER* significantly inhibited expression of the EOMES protein but not *EOMES* mRNA (Figures 6B and 6C). *CPMER* deficiency significantly reduced the differentiation efficiency of hESCs toward CMs (Figures 6D and 6E). Expression of *EEF1A2* was similarly induced at the mesoderm stage and increased along with human CM differentiation (Figure S6B). Knockdown of *EEF1A2* in hESCs significantly reduced the expression levels of key CM marker genes and the percentage of $cTNT^+$ cells compared with the control group (Figures 6F and 6G). Mechanistically, an exogenous RIP assay was employed to confirm the interaction of human *CPMER* and eEF1A2 (Figure 6H). We considered that the RNA pairing was similar between *CPMER* and *EOMES* mRNA (94–118 nt) (Figure 6I, left), which was verified by exogenous RNA pull-down assay (Figure 6I, right). Endogenous RIP results showed that enrichment of eEF1A on *EOMES* mRNAs was significantly reduced after *CPMER* knockdown (Figure 6J). Our data highlight that *CPMER* and eEF1A2 play a conserved role in regulation of *EOMES* mRNA translation and human CM differentiation.

DISCUSSION

Subtle regulation of mRNA translation is critical for controlling the expression of pivotal proteins (Roux and Topisirovic, 2018; Simpson et al., 2020). A few studies have reported that translational regulation of specific genes is closely related to protein function and heart disease. The translation efficiency of *Pabpc1* mRNA varies significantly at different stages of mouse heart development and is closely related to pathological cardiac hypertrophy (Chorghade et al., 2017). In contrast, the RNA-binding protein RBM24 prevents excessive activation of the P53 protein and diminishes heart defects by specifically inhibiting assembly of the translation initiation complex on *P53* mRNA (Zhang et al., 2018). However, the precise regulation of mRNA translation in cardiac development is not completely understood. eEF1A2, the key element of the translation complex, is specifically expressed in the heart and muscle. Previous studies have found that knockdown of *Eef1a2* causes abnormal heart development and heart failure in zebrafish, whereas deletion or mutation of *Eef1a2* leads to ataxia, muscle atrophy, and premature death in 3-week-old mice. Mutation of *Eef1a2* has also been found in individuals with dilated cardiomyopathy and growth retardation (Cao et al., 2017). These studies suggest a correlation between eEF1A2 and abnormal heart development, but the rationale is still unclear. Our results indicated that knockdown of *Eef1a2* significantly inhibits differentiation of ESCs into CMs in mice and humans by decreasing the translation efficiency of the key *Eomes* mRNA. Our study revealed, for the first time, that eEF1A2 is a conserved translation regulator in cardiac lineage commitment.

Previous studies have reported that lncRNAs often exert their exquisite regulatory functions by partnering with RNA-binding proteins. The lncRNA *UCA1* binds to PTBP1 to regulate the stability of *ALAS2* mRNA and, thus, affects heme synthesis (Liu et al., 2018). *Lnc-DC* promotes dendritic cell differentiation by binding STAT3 and protecting it from dephosphorylation (Pfeiffer et al., 2018). The eEF1A2 protein has RNA-binding capability and functions as an mRNA translation regulator, but its synergistic molecules and regulatory mechanisms remain unknown. We found that a heart-specific lncRNA, *Cpmer*, localized in the cytoplasm, interacted with eEF1A2 and significantly affected the efficiency of CM differentiation. More importantly, we also determined that the human homolog *CPMER* bound with human eEF1A2 to regulate the process of human CM differentiation. eEF1A1 and eEF1A2 proteins have nearly identical amino acid sequences, which makes it difficult to distinguish eEF1A2 from eEF1A1. So the possibility remains that *Cpmer* endogenously binds eEF1A1 and eEF1A2 to execute its regulatory function, but the precise binding specificity of *Cpmer* with eEF1A2 rather than eEF1A1 need to be explored. Our study revealed a novel function of the lncRNA *Cpmer* in regulating CM differentiation by partnering with eEF1A2 and a conserved mechanism by which the eEF1A2/*Cpmer* interaction regulates cardiac differentiation.

Heart development starts with the cardiac mesoderm, which specializes from the mesoderm, and the mesoderm

(G) Representative FACS results and the statistics of percentage of $Flk1^+Pdgfr\alpha^+$ cells. Data shown are the mean ± SEM, n = 3 independent experiments.

(H) Percentage of spontaneously contracting EBs. Data shown are the mean ± SEM, n = 3 independent experiments.

(I) qRT-PCR analysis of the CM marker genes. Data shown are the mean ± SEM, n = 3 independent experiments. *p < 0.05, **p < 0.01 (versus the WT); #p < 0.05 and ###p < 0.001 (versus KO + EV [empty vector]); Student's t test.

See also Figure S5.

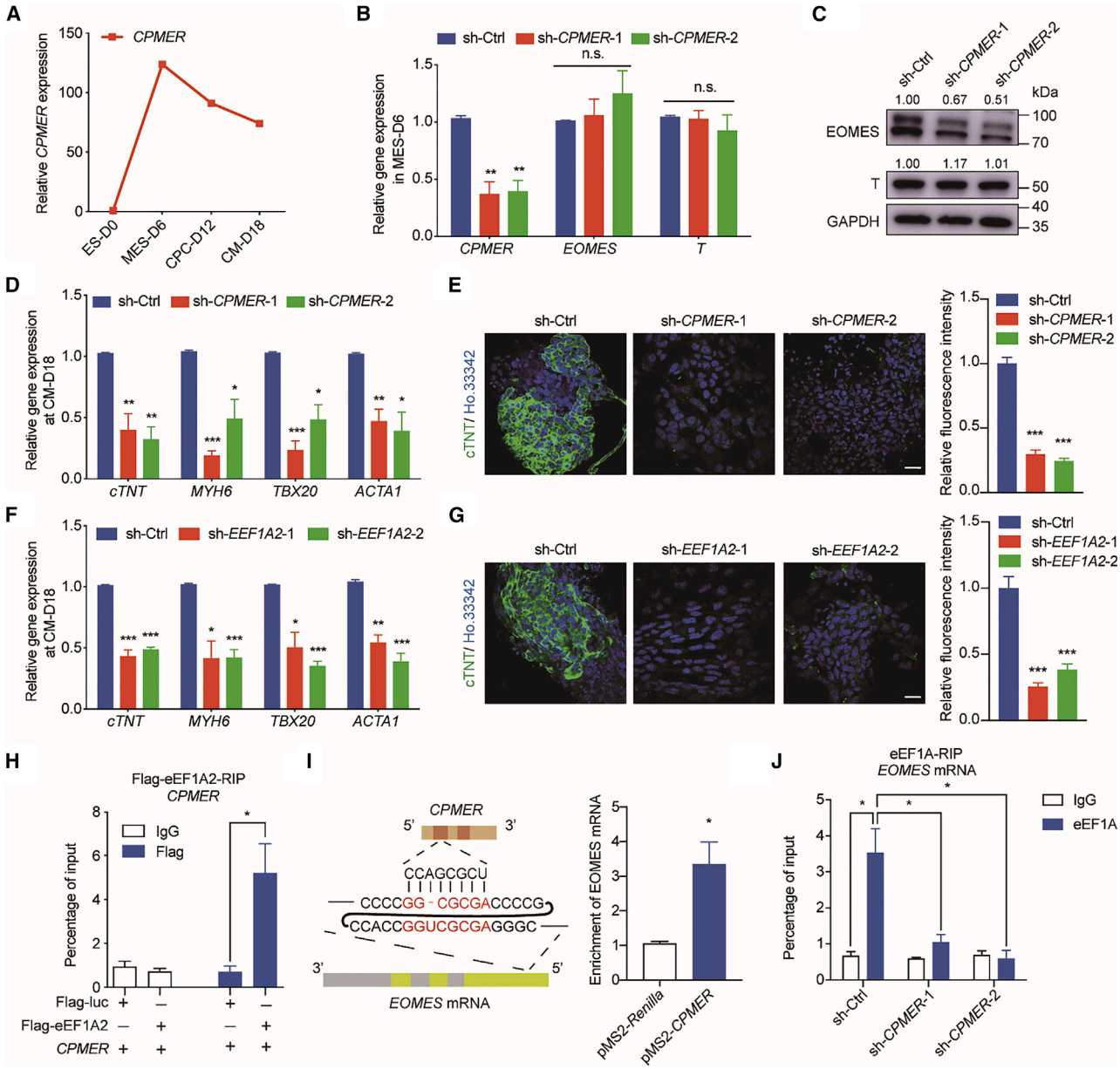

Figure 6. *CPMER*/eEF1A2 conservatively functions in *Eomes* translation and human CM differentiation

(A) Expression pattern of *CPMER* during hESC-derived CM differentiation.

(B) qRT-PCR analysis of expression of *CPMER* and mesodermal marker genes (*EOMES* and *T*) in *CPMER* knockdown cells. Data shown are the mean ± SEM, n = 3 independent experiments.

(C) Western blot analysis of EOMES and T protein levels.

(D) qRT-PCR analysis of CM marker gene expression. Data shown are the mean ± SEM, n = 3 independent experiments.

(E) cTnT immunostaining (green) on day 18 (left) and statistics for relative fluorescence intensity (right). Scale bar, 20 μm. Data shown are the mean ± SEM, n = 6 fields from 3 independent experiments.

(F) qRT-PCR analysis of CM marker gene expression. Data shown are the mean ± SEM, n = 3 independent experiments.

(G) cTnT immunostaining (green) on day 18 (left) and statistics for relative fluorescence intensity (right). Scale bar, 20 μm. Data shown are the mean ± SEM, n = 6 fields from 3 independent experiments.

(H) RIP analysis for the exogenous expression of *CPMER* and FLAG-eEF1A2 in 293T cells, determined by an anti-FLAG antibody. Data shown are the mean ± SEM, n = 3 independent experiments.

(legend continued on next page)

transcription factor EOMES plays a critical role in regulation of cardiac mesoderm specification (Costello et al., 2011; Pfeiffer et al., 2018). Deletion of *Eomes* causes significant impairment of differentiation of ESCs into CMs (van den Ameele et al., 2012). Previous studies have shown that the BMP and WNT signaling pathways activate *Eomes* transcription and that transcription factors such as NANOG (nanog homeobox), OCT4, and SOX2 also bind to the enhancer of the *Eomes* gene and activate its transcription (Arnold and Robertson, 2009; Teo et al., 2011; Tosic et al., 2019). Transcription of the *Eomes* gene is also regulated by the lncRNA *Meteor*, which is transcribed from the enhancer region of the *Eomes* gene (Alexanian et al., 2017). Only *miR-29* and *let-7* have been reported to target the 5′ UTR and open reading frame (ORF) region of *Eomes* mRNA at the post-transcriptional level, which leads to degradation of *Eomes* mRNA (Steiner et al., 2011; Wells et al., 2017). In this study, we found that *Cpmer* directly recognized *Eomes* mRNA sequences and affected the translation efficiency of *Eomes* mRNA. In-depth data revealed that *Cpmer* regulated translation of *Eomes* mainly by specifically affecting recruitment of eEF1A2 and ribosomes to *Eomes* mRNA. Our study of the precise mechanism by which *Cpmer* and eEF1A2 mediate translation regulation of *Eomes* mRNA improves our understanding of the upstream regulatory mechanisms of mRNA translation of *Eomes* in the context of cardiac development.

lncRNAs have been reported to perform their regulatory functions through RNA-RNA interactions. *HBL1*, for example, acts as a sponge of *miR-1* and inhibits differentiation of human PSCs into CMs by directly competing with the interaction of *miR-1* with its target genes (Liu et al., 2017). The lncRNA *TINCR* recognizes and affects the stability of mRNAs containing the TINCR box motif, regulating somatic tissue differentiation (Kretz et al., 2013). Recent studies have also revealed that lncRNAs can repress translation of specific genes through sequence recognition. By matching the long-length sequence of *CTNNB1* and *JUNB* mRNAs, *lincRNA-p21* leads to ribosome drop-off and inhibition of *CTNNB1* and *JUNB* mRNA translation (Yoon et al., 2012). *AS Uchl1* promotes *Uchl1* mRNA translation by facilitating assembly of the translation initiation complex (Carrieri et al., 2012). SINEUP (lncRNAs contain a SINE element and up-regulate the translation of target mRNA)-like lncRNAs enhance translation initiation of target mRNAs by acting in conjunction with PTBP1/HNRNPK (heterogeneous nuclear ribonucleoprotein K), which can serve as a potentially exogenous intervention for diseases caused by insufficient protein expression through designed artificial SINEUP lncRNAs (Bon et al., 2019). In this study, we found that the specific recognition between *Cpmer* and the *Eomes* mRNA was indispensable for translation of the *Eomes* mRNA. Deleting the recognition sequence significantly diminished binding of eEF1A2 and *Eomes* mRNAs and mRNA translation efficiency. The short recognition sequences, located at the 5′ ORF region of the *Eomes* mRNA, perhaps have a conservative responsibility for proper translation elongation. Only the *Cpmer* mutant with the ability to recognize *Eomes* mRNA and bind eEF1A2 could restore the ribosome enrichment level, EOMES protein expression, and CM differentiation. Our study revealed the novel epigenetic mechanism by which *Cpmer* mediates eEF1A2 to specifically regulate translation of *Eomes* mRNA through its dual roles of sequence recognition and protein recruitment, providing a new dimension of epigenetic regulation specificity in the research field of mRNA translation.

Our study demonstrated that the functionally conserved *Cpmer* interacted with eEF1A2 and specifically regulated translation of *Eomes* mRNA and CM differentiation. Our research on *Cpmer* not only identified a novel lncRNA capable of regulating cardiac development but also discovered a new epigenetic mechanism of lncRNA-mediated specific gene translation, which improves our knowledge of the precise post-transcriptional regulation of key transcription factors during CM differentiation.

EXPERIMENTAL PROCEDURES

A detailed description of the experimental procedures is provided in the supplemental information.

Cell culture and differentiation

46C mESCs (Aubert et al., 2003) were maintained in DMEM (Gibco) supplemented with 15% fetal bovine serum (FBS; Gibco), 1× nonessential amino acids (NEAAs; Gibco), 1× GlutaMAX (Gibco), 1× sodium pyruvate (Gibco), β-mercaptoethanol (Gibco), and leukemia inhibitory factor (LIF) on feeder cells at 37°C and 5% CO_2. Cultures were passaged every 2 days by adding 0.25% trypsin (Gibco). Mouse CM differentiation was performed as described previously (Kattman et al., 2011). H9 hESCs (WiCell) were maintained in DMEM/F12 (Gibco), 20% KO serum replacement (Gibco), 0.1 mM β-mercaptoethanol (Gibco), 1% NEAAs (Gibco), 0.5% GlutaMAX (Gibco), and 4 ng/mL hbFGF (human basic fibroblast

(I) Regions of potential recognition between *CPMER* and *EOMES* mRNA (left) and MS2bp-YFP RNA pull-down analysis for exogenous expression of pMS2-*CPMER* and human *EOMES* mRNA in 293T cells (right). Data shown are the mean ± SEM, n = 3 independent experiments.
(J) Endogenous RIP analysis for the interaction of eEF1A with *EOMES* mRNA. Data shown are the mean ± SEM, n = 3 independent experiments. *p < 0.05, **p < 0.01, ***p < 0.001 (versus sh-Ctrl); Student's t test.
See also Figure S6.

growth factor) (R&D Systems) on a feeder layer. hESC-induced CM differentiation was performed as described previously (Protze et al., 2017).

Vectors

shRNAs targeting Eef1a2 (mouse and human), Eomes (mouse), and *Cpmer* (mouse and human) were designed and inserted into the pLKO.1 vector (Addgene). The cDNA fragments corresponding to the RACE findings on *Cpmer* were cloned into the donor vector (introduced into the Rosa26 locus of mESCs), pBSK vector, and pMS2 vector (Addgene), respectively. *Cpmer* E1, E2, E3, E12, E23, and E13 transcripts; the FL and deletion mutant *Eomes* (GenBank: NM_010136) sequences; *Eomes* sequences; and GFP fusion reporter sequences were cloned into the Fugw vector (Addgene). All constructed plasmids were verified by DNA sequencing. All primer sequences are listed in Table S4.

Biotin-RNA pull-down and liquid chromatography (LC)-mass spectrometry (MS)

Biotin-labeled *Cpmer* was obtained using RNA Labeling Mix (11685597910, Roche) with T7 (10881767001, Roche) or T3 RNA polymerase (11031171001, Roche). Total RNA was heated to 90°C for 2 min, held on ice for 2 min, and incubated in RNA structure buffer. Lysis was performed using streptavidin beads coated with biotin-labeled sense *Cpmer* or antisense *Cpmer*. The RNA-binding proteins were analyzed by LC-MS as described previously (Shevchenko et al., 2006).

RIP and MS2bp-YFP RNA pull-down assay

RIP and MS2bp-YFP-based RNA pull-down assays were performed as described previously (Ng et al., 2012). The eEF1A antibody was able to endogenously recognize eEF1A1 and eEF1A2 proteins.

Polysome profile analysis

Polysome profile analysis was performed as described previously (Panda et al., 2017). The eEF1A antibody was able to recognize eEF1A1 and eEF1A2 in the co-sedimenting protein of polysomes.

Statistical analysis

Statistical significance was analyzed with two-tailed Student's t test from three independent experiments. Mean values ±SEM are shown.

Data and code availability

All data are available in the main text or the supplemental information. Additional data related to this paper may be requested from the lead contact. The MS proteomics data are available via ProteomeXchange with identifier ProteomeXchange: PXD031814. Datasets have been deposited in the Gene Expression Omnibus Database under accession number GSE158202.

SUPPLEMENTAL INFORMATION

Supplemental information can be found online at https://doi.org/10.1016/j.stemcr.2022.03.006.

AUTHOR CONTRIBUTIONS

Y.L., X.G., and J.K. designed the study and wrote the manuscript. Y.L., X.Z., and Y.X. performed the experiments and data analyses. W.J. and Y.W. contributed to the interpretation of data. All authors approved the final version of the manuscript.

CONFLICTS OF INTEREST

The authors declare no competing interests.

ACKNOWLEDGMENTS

This study was supported by grants from the Ministry of Science and Technology (2018YFA0800100), the National Natural Science Foundation of China (31830059, 31970599, 32170575, 31871298, 31721003, and 32000605), the Shanghai Rising-Star Program (20QA1409600), and the Fundamental Research Funds for the Central Universities (22120220104).

Received: October 1, 2021
Revised: March 7, 2022
Accepted: March 8, 2022
Published: April 7, 2022

REFERENCES

Alexanian, M., Maric, D., Jenkinson, S.P., Mina, M., Friedman, C.E., Ting, C.C., Micheletti, R., Plaisance, I., Nemir, M., Maison, D., et al. (2017). A transcribed enhancer dictates mesendoderm specification in pluripotency. Nat. Commun. *8*, 1806.

Amita, M., Adachi, K., Alexenko, A.P., Sinha, S., Schust, D.J., Schulz, L.C., Roberts, R.M., and Ezashi, T. (2013). Complete and unidirectional conversion of human embryonic stem cells to trophoblast by BMP4. Proc. Natl. Acad. Sci. U S A *110*, E1212–E1221.

Anderson, K.M., Anderson, D.M., McAnally, J.R., Shelton, J.M., Bassel-Duby, R., and Olson, E.N. (2016). Transcription of the non-coding RNA upperhand controls Hand2 expression and heart development. Nature *539*, 433–436.

Arnold, S.J., and Robertson, E.J. (2009). Making a commitment: cell lineage allocation and axis patterning in the early mouse embryo. Nat. Rev. Mol. Cell Biol. *10*, 91–103.

Aubert, J., Stavridis, M.P., Tweedie, S., O'Reilly, M., Vierlinger, K., Li, M., Ghazal, P., Pratt, T., Mason, J.O., Roy, D., and Smith, A. (2003). Screening for mammalian neural genes via fluorescence-activated cell sorter purification of neural precursors from Sox1-gfp knock-in mice. Proc. Natl. Acad. Sci. U S A *100* (*Suppl 1*), 11836–11841.

Bon, C., Luffarelli, R., Russo, R., Fortuni, S., Pierattini, B., Santulli, C., Fimiani, C., Persichetti, F., Cotella, D., Mallamaci, A., et al. (2019). SINEUP non-coding RNAs rescue defective frataxin expression and activity in a cellular model of Friedreich's Ataxia. Nucleic Acids Res. *47*, 10728–10743.

Cao, S., Smith, L.L., Padilla-Lopez, S.R., Guida, B.S., Blume, E., Shi, J., Morton, S.U., Brownstein, C.A., Beggs, A.H., Kruer, M.C., and Agrawal, P.B. (2017). Homozygous EEF1A2 mutation causes dilated

cardiomyopathy, failure to thrive, global developmental delay, epilepsy and early death. Hum. Mol. Genet. *26*, 3545–3552.

Carrieri, C., Cimatti, L., Biagioli, M., Beugnet, A., Zucchelli, S., Fedele, S., Pesce, E., Ferrer, I., Collavin, L., Santoro, C., et al. (2012). Long non-coding antisense RNA controls Uchl1 translation through an embedded SINEB2 repeat. Nature *491*, 454–457.

Chang, C.P., and Bruneau, B.G. (2012). Epigenetics and cardiovascular development. Annu. Rev. Physiol. *74*, 41–68.

Chorghade, S., Seimetz, J., Emmons, R., Yang, J., Bresson, S.M., Lisio, M., Parise, G., Conrad, N.K., and Kalsotra, A. (2017). Poly(A) tail length regulates PABPC1 expression to tune translation in the heart. Elife *6*, e24139.

Costello, I., Pimeisl, I.-M., Dräger, S., Bikoff, E.K., Robertson, E.J., and Arnold, S.J. (2011). The T-box transcription factor Eomesodermin acts upstream of Mesp1 to specify cardiac mesoderm during mouse gastrulation. Nat. Cell Biol. *13*, 1084–1091.

Frank, S., Ahuja, G., Bartsch, D., Russ, N., Yao, W., Kuo, J.C.-C., Derks, J.-P., Akhade, V.S., Kargapolova, Y., Georgomanolis, T., et al. (2019). yylncT defines a class of divergently transcribed lncRNAs and safeguards the T-mediated mesodermal commitment of human PSCs. Cell Stem Cell *24*, 318–327.e8.

Fujii, K., Shi, Z., Zhulyn, O., Denans, N., and Barna, M. (2017). Pervasive translational regulation of the cell signalling circuitry underlies mammalian development. Nat. Commun. *8*, 14443.

Fukunaga, T., and Hamada, M. (2017). RIblast: an ultrafast RNA-RNA interaction prediction system based on a seed-and-extension approach. Bioinformatics *33*, 2666–2674.

Galceran, J., Farinas, I., Depew, M.J., Clevers, H., and Grosschedl, R. (1999). Wnt3a-/–like phenotype and limb deficiency in Lef1(-/-) Tcf1(-/-) mice. Genes Dev. *13*, 709–717.

Gibb, E.A., Brown, C.J., and Lam, W.L. (2011). The functional role of long non-coding RNA in human carcinomas. Mol. Cancer *10*, 38.

Guo, X., Xu, Y., Wang, Z., Wu, Y., Chen, J., Wang, G., Lu, C., Jia, W., Xi, J., Zhu, S., et al. (2018). A linc1405/Eomes complex promotes cardiac mesoderm specification and cardiogenesis. Cell Stem Cell *22*, 893–908.e6.

Hosen, M.R., Militello, G., Weirick, T., Ponomareva, Y., Dassanayaka, S., Moore, J.B.t., Doring, C., Wysoczynski, M., Jones, S.P., Dimmeler, S., and Uchida, S. (2018). Airn regulates Igf2bp2 translation in cardiomyocytes. Circ. Res. *122*, 1347–1353.

Johansson, B.M., and Wiles, M.V. (1995). Evidence for involvement of activin A and bone morphogenetic protein 4 in mammalian mesoderm and hematopoietic development. Mol. Cell. Biol. *15*, 141–151.

Kattman, S.J., Witty, A.D., Gagliardi, M., Dubois, N.C., Niapour, M., Hotta, A., Ellis, J., and Keller, G. (2011). Stage-specific optimization of activin/nodal and BMP signaling promotes cardiac differentiation of mouse and human pluripotent stem cell lines. Cell Stem Cell *8*, 228–240.

Kretz, M., Siprashvili, Z., Chu, C., Webster, D.E., Zehnder, A., Qu, K., Lee, C.S., Flockhart, R.J., Groff, A.F., Chow, J., et al. (2013). Control of somatic tissue differentiation by the long non-coding RNA TINCR. Nature *493*, 231–235.

Liu, J., Li, Y., Lin, B., Sheng, Y., and Yang, L. (2017). HBL1 is a human long noncoding RNA that modulates cardiomyocyte development from pluripotent stem cells by counteracting MIR1. Dev. Cell *42*, 333–348.e5.

Liu, J., Li, Y., Tong, J., Gao, J., Guo, Q., Zhang, L., Wang, B., Zhao, H., Wang, H., Jiang, E., et al. (2018). Long non-coding RNA-dependent mechanism to regulate heme biosynthesis and erythrocyte development. Nat. Commun. *9*, 4386.

Liu, S., Hausmann, S., Carlson, S.M., Fuentes, M.E., Francis, J.W., Pillai, R., Lofgren, S.M., Hulea, L., Tandoc, K., Lu, J., et al. (2019). METTL13 methylation of eEF1A increases translational output to promote tumorigenesis. Cell *176*, 491–504.e21.

Miura, P., Coriati, A., Belanger, G., De Repentigny, Y., Lee, J., Kothary, R., Holcik, M., and Jasmin, B.J. (2010). The utrophin A 5′-UTR drives cap-independent translation exclusively in skeletal muscles of transgenic mice and interacts with eEF1A2. Hum. Mol. Genet. *19*, 1211–1220.

Monteiro, R.M., de Sousa Lopes, S.M., Korchynskyi, O., ten Dijke, P., and Mummery, C.L. (2004). Spatio-temporal activation of Smad1 and Smad5 in vivo: monitoring transcriptional activity of Smad proteins. J. Cell Sci. *117*, 4653–4663.

Moore-Morris, T., van Vliet, P.P., Andelfinger, G., and Puceat, M. (2018). Role of epigenetics in cardiac development and congenital diseases. Physiol. Rev. *98*, 2453–2475.

Mullin, N.K., Mallipeddi, N.V., Hamburg-Shields, E., Ibarra, B., Khalil, A.M., and Atit, R.P. (2017). Wnt/beta-catenin signaling pathway regulates specific lncRNAs that impact dermal fibroblasts and skin fibrosis. Front. Genet. *8*, 183.

Murry, C.E., and Keller, G. (2008). Differentiation of embryonic stem cells to clinically relevant populations: lessons from embryonic development. Cell *132*, 661–680.

Ng, S.Y., Johnson, R., and Stanton, L.W. (2012). Human long noncoding RNAs promote pluripotency and neuronal differentiation by association with chromatin modifiers and transcription factors. EMBO J. *31*, 522–533.

Oosterwegel, M., van de Wetering, M., Timmerman, J., Kruisbeek, A., Destree, O., Meijlink, F., and Clevers, H. (1993). Differential expression of the HMG box factors TCF-1 and LEF-1 during murine embryogenesis. Development *118*, 439–448.

Ounzain, S., Micheletti, R., Beckmann, T., Schroen, B., Alexanian, M., Pezzuto, I., Crippa, S., Nemir, M., Sarre, A., Johnson, R., et al. (2015). Genome-wide profiling of the cardiac transcriptome after myocardial infarction identifies novel heart-specific long non-coding RNAs. Eur. Heart J. *36*, 353–368a.

Panda, A.C., Martindale, J.L., and Gorospe, M. (2017). Polysome fractionation to analyze mRNA distribution profiles. Bio Protoc. *7*, e2126.

Pfeiffer, M.J., Quaranta, R., Piccini, I., Fell, J., Rao, J., Ropke, A., Seebohm, G., and Greber, B. (2018). Cardiogenic programming of human pluripotent stem cells by dose-controlled activation of EOMES. Nat. Commun. *9*, 440.

Protze, S.I., Liu, J., Nussinovitch, U., Ohana, L., Backx, P.H., Gepstein, L., and Keller, G.M. (2017). Sinoatrial node cardiomyocytes derived from human pluripotent cells function as a biological pacemaker. Nat. Biotechnol. *35*, 56–68.

Roux, P.P., and Topisirovic, I. (2018). Signaling pathways involved in the regulation of mRNA translation. Mol. Cell. Biol. *38*, e00070-18.

Shevchenko, A., Tomas, H., Havlis, J., Olsen, J.V., and Mann, M. (2006). In-gel digestion for mass spectrometric characterization of proteins and proteomes. Nat. Protoc. *1*, 2856–2860.

Simpson, L.J., Reader, J.S., and Tzima, E. (2020). Mechanical regulation of protein translation in the cardiovascular system. Front. Cell Dev. Biol. *8*, 34.

Soares, M.L., Haraguchi, S., Torres-Padilla, M.E., Kalmar, T., Carpenter, L., Bell, G., Morrison, A., Ring, C.J., Clarke, N.J., Glover, D.M., and Zernicka-Goetz, M. (2005). Functional studies of signaling pathways in peri-implantation development of the mouse embryo by RNAi. BMC Dev. Biol. *5*, 28.

Steiner, D.F., Thomas, M.F., Hu, J.K., Yang, Z., Babiarz, J.E., Allen, C.D., Matloubian, M., Blelloch, R., and Ansel, K.M. (2011). MicroRNA-29 regulates T-box transcription factors and interferon-gamma production in helper T cells. Immunity *35*, 169–181.

Teo, A.K.K., Arnold, S.J., Trotter, M.W.B., Brown, S., Ang, L.T., Chng, Z., Robertson, E.J., Dunn, N.R., and Vallier, L. (2011). Pluripotency factors regulate definitive endoderm specification through eomesodermin. Genes Dev. *25*, 238–250.

Tosic, J., Kim, G.J., Pavlovic, M., Schroder, C.M., Mersiowsky, S.L., Barg, M., Hofherr, A., Probst, S., Kottgen, M., Hein, L., and Arnold, S.J. (2019). Eomes and Brachyury control pluripotency exit and germ-layer segregation by changing the chromatin state. Nat. Cell Biol. *21*, 1518–1531.

van den Ameele, J., Tiberi, L., Bondue, A., Paulissen, C., Herpoel, A., Iacovino, M., Kyba, M., Blanpain, C., and Vanderhaeghen, P. (2012). Eomesodermin induces Mesp1 expression and cardiac differentiation from embryonic stem cells in the absence of Activin. EMBO Rep. *13*, 355–362.

Wells, A.C., Daniels, K.A., Angelou, C.C., Fagerberg, E., Burnside, A.S., Markstein, M., Alfandari, D., Welsh, R.M., Pobezinskaya, E.L., and Pobezinsky, L.A. (2017). Modulation of let-7 miRNAs controls the differentiation of effector CD8 T cells. Elife *6*, e26398.

Wilusz, J.E., Sunwoo, H., and Spector, D.L. (2009). Long noncoding RNAs: functional surprises from the RNA world. Genes Dev. *23*, 1494–1504.

Xing, S., Gai, K., Li, X., Shao, P., Zeng, Z., Zhao, X., Zhao, X., Chen, X., Paradee, W.J., Meyerholz, D.K., et al. (2019). Tcf1 and Lef1 are required for the immunosuppressive function of regulatory T cells. J. Exp. Med. *216*, 847–866.

Yoon, J.H., Abdelmohsen, K., Srikantan, S., Yang, X., Martindale, J.L., De, S., Huarte, M., Zhan, M., Becker, K.G., and Gorospe, M. (2012). LincRNA-p21 suppresses target mRNA translation. Mol. Cell *47*, 648–655.

Zhang, M., Zhang, Y., Xu, E., Mohibi, S., de Anda, D.M., Jiang, Y., Zhang, J., and Chen, X. (2018). Rbm24, a target of p53, is necessary for proper expression of p53 and heart development. Cell Death Differ. *25*, 1118–1130.

Stem Cell Reports, Volume *17*

Supplemental Information

Cpmer: A new conserved eEF1A2-binding partner that regulates *Eomes* translation and cardiomyocyte differentiation

Yao Lyu, Wenwen Jia, Yukang Wu, Xin Zhao, Yuchen Xia, Xudong Guo, and Jiuhong Kang

Supplemental Information

Supplemental Figures and Legends:

Figure S1. Identification of *Cpmer* as a non-coding RNA. Related to figure 1.

Figure S2. The effect of *Cpmer* on the expression of pluripotent genes, neighbor gene, and lineage genes. Related to figure 2.

Figure S3. *Cpmer* specifically affects the translation of Eomes, which is critical for the CM differentiation, independent of the eEF1A recruitment in ribosome complex. Related to figure 4.

Figure S4. Single exon of *Cpmer* is not able to rescue the EOMES expression or CM differentiation. Related to figure 5.

Figure S5. Knockdown of *Cpmer* after mesoderm stage also inhibits the CM differentiation. Related to figure 5.

Figure S6. Expression patterns of stage-specific markers and *EEF1A2* gene during hESC-derived CM differentiation. Related to figure 6.

Supplemental Tables:

Table S1. Sequence information of de novo lncRNAs. Related to figure 1.

Table S2. Protein identification results for Biotin-labeled *Cpmer* RNA pull-down experiments. Related to figure 3.

Table S3. RIblast ris result. Related to figure 4.

Table S4. Primers used for vector construction.

Table S5. Primers used in qRT-PCR.

Table S6. Antibodies used in the study.

Supplemental Experimental Procedures

Supplementary Data of Whole Membrane Image

Supplemental Figures and Legends:

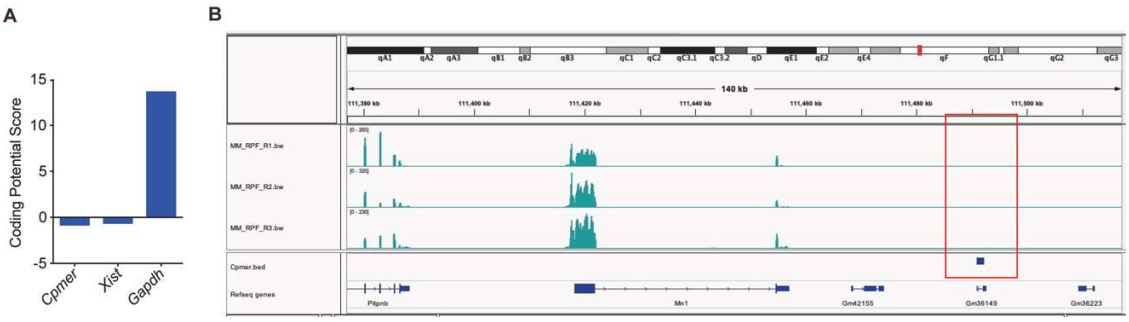

Figure S1. Identification of *Cpmer* as a non-coding RNA. Related to figure 1.

(A) The coding potential prediction of *Cpmer*, *Xist*, and *Gapdh* by Coding Potential Calculator (http://cpc.gao-lab.org).

(B) The ribosome occupancy analysis of the *Cpmer* and *Mn1* mRNA in mesoderm cells (GSE86467).

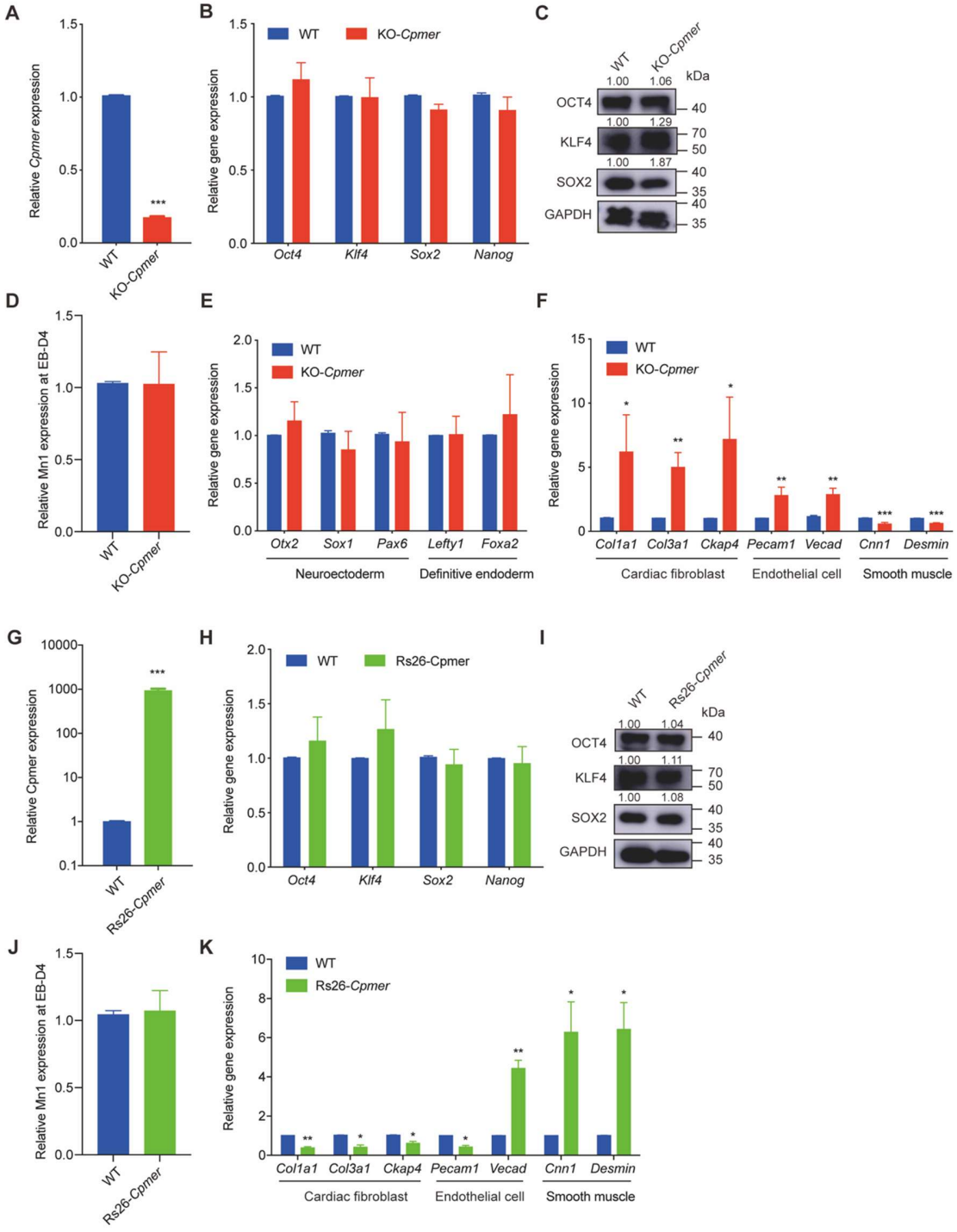

Figure S2. The effect of *Cpmer* on the expression of pluripotent genes, neighbor gene, and lineage genes. Related to figure 2.

(A-B) qRT-PCR analysis of the expression of *Cpmer* and pluripotency-related genes in KO-*Cpmer* ESCs compared with WT ESCs. Data shown are the mean ± SEM, n=3 independent experiments.

(C) Western blotting analysis of pluripotency-related gene expression in WT and KO-*Cpmer* ESCs.

(D) qRT-PCR analysis of *Mn1* expression in KO-*Cpmer* MES cells compared with WT cells. Data shown are the mean ± SEM, n=3 independent experiments.

(E) qRT-PCR analysis of the expression of neuroectoderm markers (*Otx2*, *Sox1*, and *Pax6*) and definitive endoderm markers (*Lefty1* and *Foxa2*) in KO-*Cpmer* cells compared with WT cells. Data shown are the mean ± SEM, n=3 independent experiments.

(F) qRT-PCR analysis of the expression of cardiac fibroblast markers (*Col1a1*, *Col3a1*, and *Ckap4*), endothelial cell markers (*Pecam1* and *Vecad*), and smooth muscle markers (*Cnn1* and *Desmin*) in KO-*Cpmer* cells compared with WT cells. Data shown are the mean ± SEM, n=3 independent experiments.

(G-H) qRT-PCR analysis of the expression of *Cpmer* or pluripotency-related genes in Rs26-*Cpmer* ESCs compared with WT ESCs. Data shown are the mean ± SEM, n=3 independent experiments.

(I) Western blotting analysis of pluripotency-related gene expression in WT and Rs26-*Cpmer* ESCs.

(J) qRT-PCR analysis of *Mn1* expression in Rs26-*Cpmer* MES cells compared with WT cells. Data shown are the mean ± SEM, n=3 independent experiments.

(K) qRT-PCR analysis of the expression of cardiac fibroblast markers, endothelial cell markers, and smooth muscle markers in Rs26-*Cpmer* cells compared with WT cells. Data shown are the mean ± SEM, n=3 independent experiments.

*P < 0.05, **P < 0.01, and ***P < 0.001 (versus WT) by Student`s t-test.

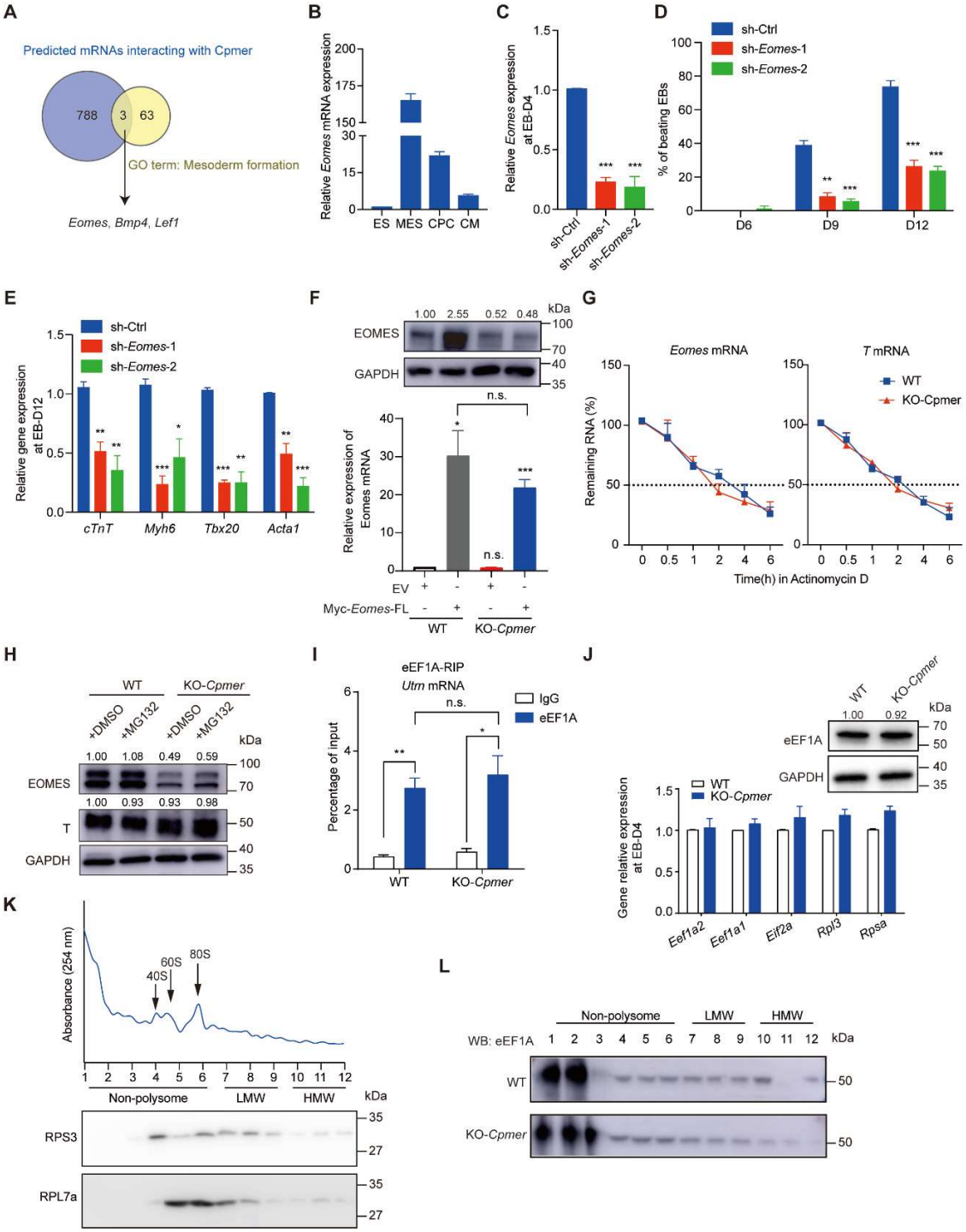

Figure S3. *Cpmer* specifically affects the translation of Eomes, which is critical for the CM differentiation, independent of the eEF1A recruitment in ribosome complex. Related to figure 4.

(A) Overlapping of the predicted mRNAs (791) interacted with *Cpmer* and the genes (66) associated with mesoderm formation (GO_ID: 00010707).

(B) The expression pattern of *Eomes* during CM differentiation. Data shown are mean ± SEM, n=3 independent experiments.

(C) The expression of *Eomes* at day 4 of EB differentiation after *Eomes* knockdown (sh-*Eomes*-1 and sh-*Eomes*-2) in ESCs. Data shown are mean ± SEM, n=3 independent experiments.

(D) Percentage of spontaneously contracting EBs determined at days 6, 9, and 12 of EB differentiation in *Eomes* knockdown cells compared with control cells. Data shown are mean ± SEM, n=3 independent experiments.

(E) qRT-PCR analysis of the CM marker genes in *Eomes* knockdown cells compared with control cells at day 12 of EB differentiation. Data shown are mean ± SEM, n=3 independent experiments.

(F) qRT-PCR and western blot analysis of *Eomes* mRNA and protein levels in the WT and KO-*Cpmer* cells transfected with full-length (FL) *Eomes* at the mesoderm stage. Data shown are mean ± SEM, n=3 independent experiments.

(G) The half-lives of *Eomes* and *T* mRNA were quantified after exposure to actinomycin D at different time points (0, 0.5, 1, 2, 4, and 6 h). Data shown are the mean ± SEM, n=3 independent experiments.

(H) Western blotting analysis of EOMES and T protein levels in the WT and KO-*Cpmer* mesoderm cells after treatment with MG132 (5 μM) for 6 h.

(I) Endogenous RIP analysis of the interaction of eEF1A with *Utrn* mRNA (as positive control) in the WT and KO-*Cpmer* cells at the mesoderm stage. Data shown are mean ± SEM, n=3 independent experiments.

(J) qRT-PCR and western blotting analysis of translation-related genes in the WT and KO-*Cpmer* cells at day 4 of EB differentiation (EB-D4). Data shown are mean ± SEM, n=3 independent experiments.

(K) Polysome trace analysis exhibited the presence of absorption peaks for free RNA, pre-polysome (40S, 60S, and 80S), and polysomes (LMW and HMW) (up) and the accompanying western blotting of RPS3 (40S ribosomal protein S3) and RPL7a (60S ribosomal protein L7a) (down).

(L) Western blotting analysis of eEF1A distribution in polysome fractions of the WT and KO-*Cpmer* cells at EB-D4.

*P < 0.05, **P < 0.01, and ***P < 0.001 (versus sh-Ctrl) by Student`s t-test.

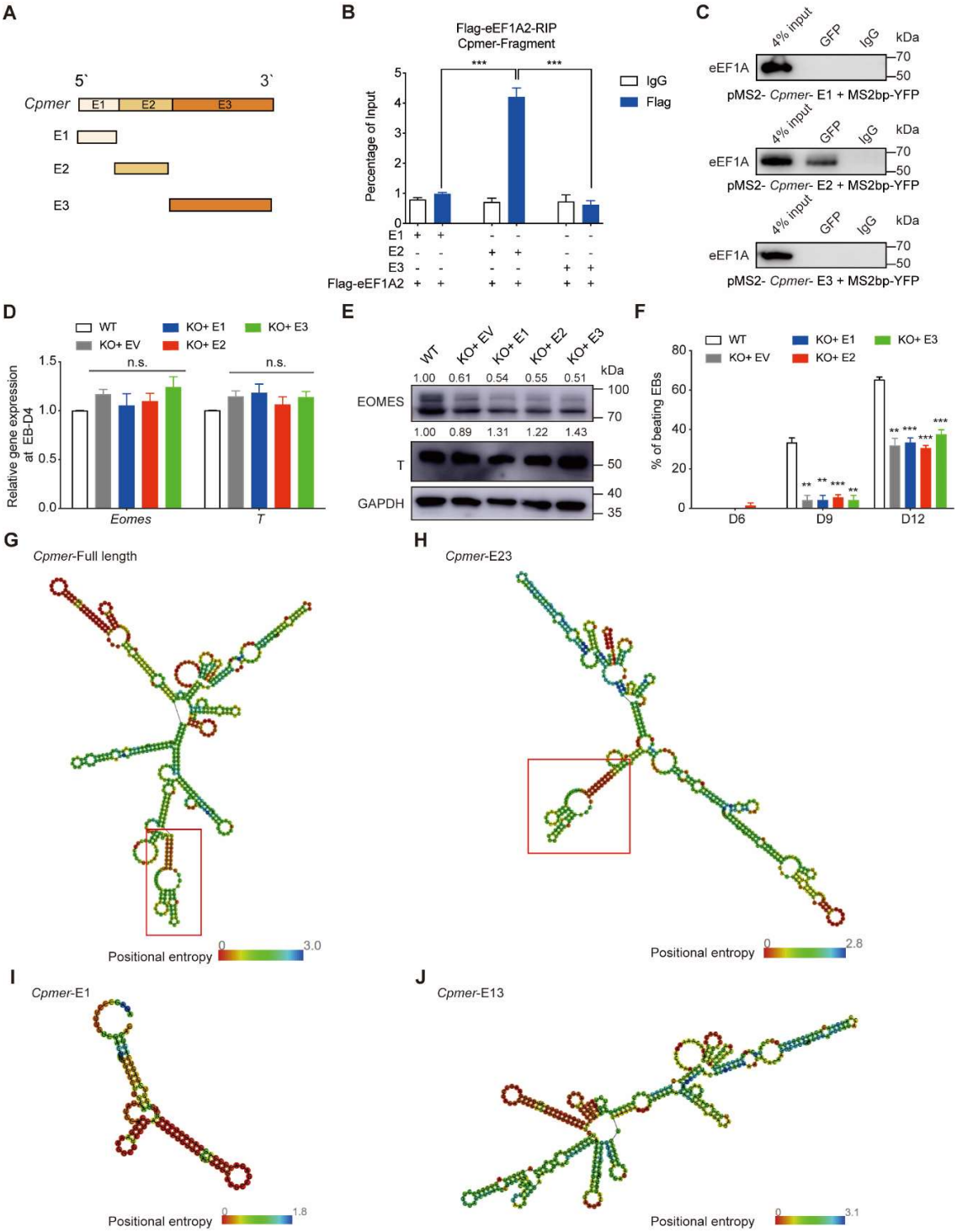

Figure S4. Single exon of *Cpmer* is not able to rescue the EOMES expression or CM differentiation.

Related to figure 5.

(A) Schematic representation of the full-length *Cpmer* and three mutants (single exons: E1, E2, and E3).

(B) RIP analysis for the exogenous expression of *Cpmer* mutants and Flag-eEF1A2 in 293T cells, as determined by anti-Flag antibody.

(C) MS2bp-YFP RNA pull-down analysis for mesoderm cells co-transfected with MS2-*Cpmer* mutants and MS2bp-YFP.

(D-E) qRT-PCR and western blotting analysis of *Eomes* and *T* expression in the KO-*Cpmer* cells transfected with different *Cpmer* mutants at mesoderm stage.

(F) Percentage of spontaneously contracting EBs in the WT and KO-*Cpmer* cells transfected with different *Cpmer* mutants.

Data shown are the mean ± SEM (n=3). **P < 0.01 and ***P < 0.001 (versus WT) by Student`s t-test.

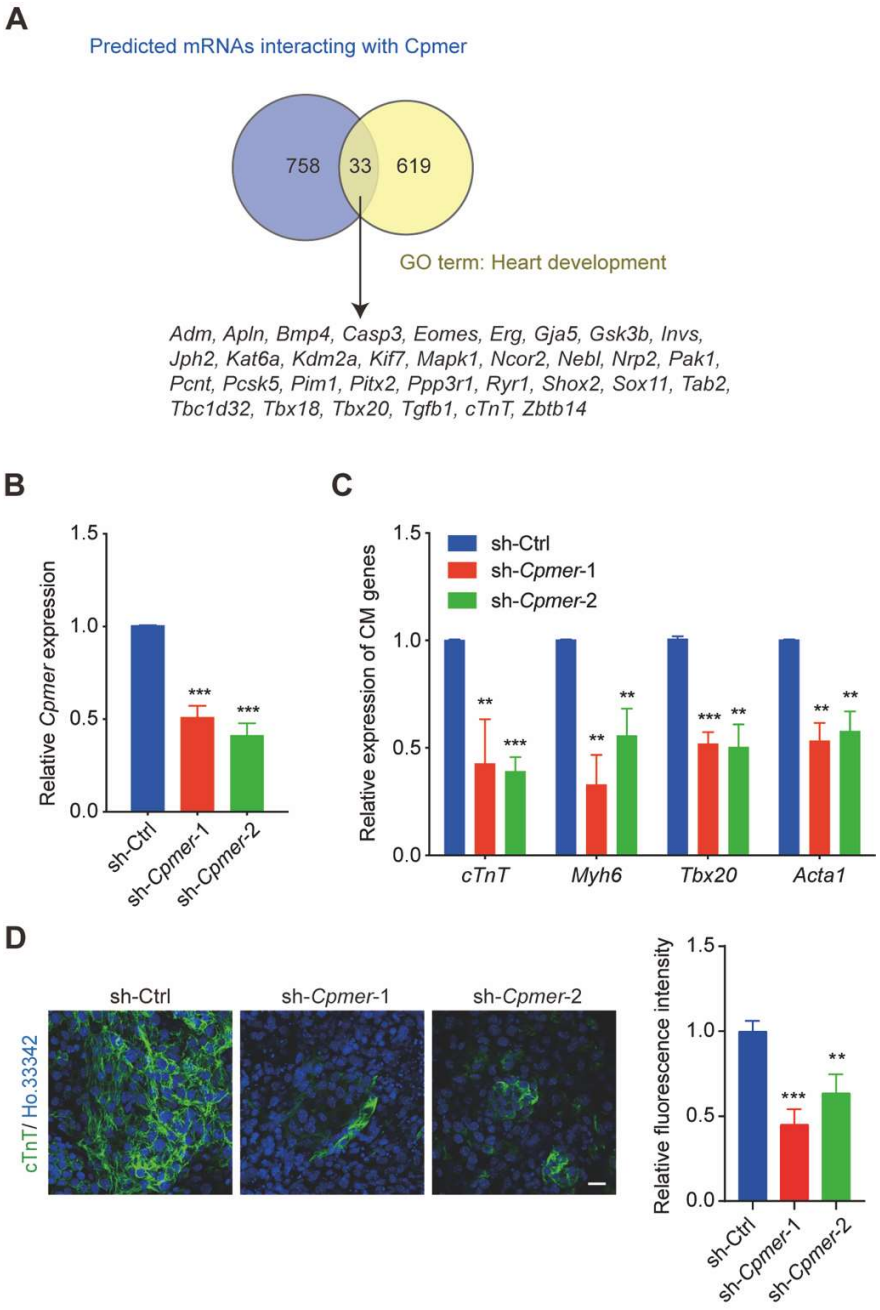

Figure S5. Knockdown of *Cpmer* after mesoderm stage also inhibits the CM differentiation. Related to figure 5.

(A) Overlapping of the predicted mRNAs (791) interacted with *Cpmer* and the genes (622) associated with heart development (GO_ID:0007507).

(B) The expression detection of *Cpmer* knockdown with shRNA virus (sh-*Cpmer*-1 and sh-*Cpmer*-2) after mesoderm stage. Data shown are mean ± SEM, n=3 independent experiments.

(C) qRT-PCR analysis of the CM marker genes in the *Cpmer* knockdown cells compared with control cells at day 8 of CM differentiation. Data shown are mean ± SEM, n=3 independent experiments.

(D) cTnT immunostaining (green) in the *Cpmer* knockdown and control cells at day 8 of CM differentiation (left). The statistics for relative fluorescence intensity was shown (right). Scale bar, 20 μm. Data shown are the mean ± SEM (n= 6 fields from 3 independent experiments).

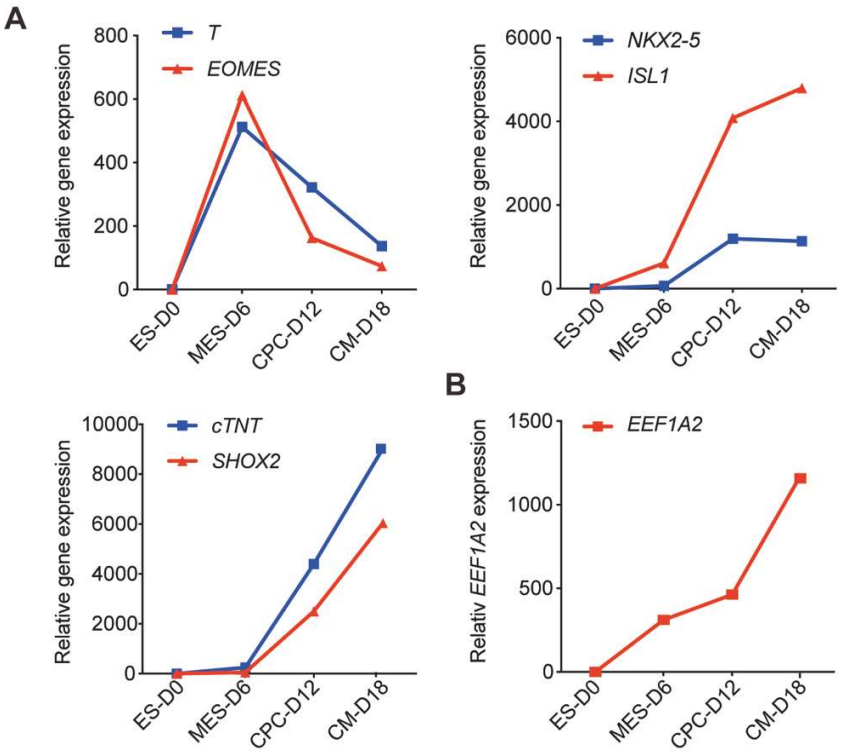

Figure S6. Expression patterns of stage-specific markers and *EEF1A2* gene during hESC-derived CM differentiation. Related to figure 6.

(A) qRT-PCR analysis of marker genes at the indicated stages (ES, MES, CPC, and CM) of hESC-derived CM differentiation.

(B) Expression pattern of *EEF1A2* during hESC-derived CM differentiation.

Supplemental Experimental Procedures

Cell culture and differentiation

For EB differentiation, mESCs were plated at a density of 4×10^4 cells/mL in ultralow-attachment plates in 5 mL of mESC medium without LIF. The medium was changed every 2 days. For beating EB analysis, single EBs were picked and reseeded onto gelatin-coated 48-well plates on the 4th day. Beating EBs were observed under a light microscope from the 6th day to the 12th day.

For mouse CM differentiation, mESCs were cultured in serum-free medium (DMEM: Neurobasal=1:1 (v/v) (Gibco), 0.05% BSA, 2 mM GlutaMAX, 0.5 × N2 supplement (Gibco), 0.5×B27 supplement (Gibco), 1.5×10^{-4} M monothioglycerol, 10 ng/mL hBMP4 (R&D), and LIF (Millipore; 10000×)) for 2 passages. The medium was changed every day. Then, EBs were aggregated at a density of 6×10^4 cells/mL for 48 h in serum-free medium (DMEM: DMEM/Ham's F12=1:1 (v/v) (Gibco), 0.05% BSA, 2 mM GlutaMAX, 1 × N2 supplement, 1×B27 supplement, 4.5×10^{-4} M monothioglycerol, and 25 μg/ml L-ascorbic acid (Sigma-Aldrich)). EBs were dissociated with 0.125% trypsin and reaggregated in the presence of 0.2 ng/mL hBMP4, 5 ng/mL hVEGF (R&D), 5 ng/mL hActivin A (R&D), and 25 μg/mL L-ascorbic acid for 40 h. EBs were dissociated and plated in gelatin-coated 12-well plates at a density of 2.5×10^5 cells/well with StemPro-34 medium (Gibco) supplemented with 5 ng/mL hVEGF, 10 ng/mL hbFGF (R&D), 25 ng/mL hFGF10 (R&D), and 25 μg/ml L-ascorbic acid. The medium was changed every day until contracting CMs were observed.

For hESCs induced CM differentiation, hESCs were incubated with dispase (Gibco) at 37°C for 5 mins. Then, colonies were cultured in suspension as EBs in basic StemPro-34 (Gibco) media for 18 h in ultra-low attachments dishes. At day 1, EBs were cultured in pacemaker mesoderm induction media. At day 3, EBs were harvested and washed once then cultured in cardiac induction media. At day 6, media was changed to cardiac maintenance media, and the media was changed every 3 days until day 18.

RNA-sequencing and bioinformatic analysis

The whole heart samples were collected from embryos at E10.5, E14.5, E17.5, as well as the newborn and adult mice. Total RNA for RNA-seq analysis was isolated from the heart samples using RNAiso Reagent (TaKaRa) and paired-end RNA-seq for developing mouse hearts was performed. The RNA-seq reads of developing hearts were aligned to the mm9 UCSC reference gene GTF using TopHat2 with default parameters. The transcript assembly and differential expression analysis with the mm9 UCSC reference gene GTF and reference genome GSE52313 were performed through Cufflinks2 and Cuffdiff2 with default parameters, respectively. The upregulated lncRNAs were sorted by the changes in FPKM during heart development.

Generation of Cpmer-knockout cell lines

A dual guide RNA (gRNA) knockout strategy was used to completely knock out *Cpmer*. The gRNAs targeted to the 5' and 3' regions of *Cpmer* were designed by using the CRISPR DESIGN website (https://zlab.bio/guide-design-resources), and the detailed sequences are shown in Table S4. The gRNAs were inserted into the pX330 vector. Two gRNAs and Cas9 plasmids of 5 μg each were mixed in P3 primary Cell Solution Box (PBP3-00675, Lonza), electroporated into mESCs with the Gene Pulser X Cell System (Bio-Rad) at 250 V and 500 μF in a 0.4 cm Gene Pulser cuvette (Bio-Rad), and then seeded on feeder cells. 24 h later, 0.5 μg/mL puromycin was added for 2 days. Individual colonies were picked and expanded in 24-well plates with feeder cells. The genomic DNA from each colony was extracted by a TIANamp Genomic DNA Kit (DP304-03) and further verified by PCR.

RACE

To obtain the full-length sequence of the *Cpmer* transcript, 5 prime and 3 prime RACE methods were employed to amplify the cDNA of mouse heart tissue using the SMARTer RACE 5'/3' Kit (TaKaRa). cDNA with adapter addition was cloned into the pPLB vector (TIANGEN) and verified by sequencing. The sequences of gene-specific primers are listed in Table S4.

Flow cytometry and cell sorting

EBs generated from CM differentiation experiments at day 4 were dissociated with 0.125% trypsin (Gibco) and washed with 1× PBS. The dissociated cells were stained with 1 μL of CD140a (Pdgfrα)-APC antibody (130-109-784, Miltenyi Biotec.) and 1 μL of CD309 (Flk1)-PE antibody (130-102-559, Miltenyi Biotec.) for 30 min at room temperature. Then, the cells were washed with 1×PBS and analyzed by BD FACSVerse and FlowJo software.

Biotin-RNA pull-down and LC-MS

Biotin-labeled *Cpmer* was obtained using RNA Labeling Mix (11685597910, Roche) with T7 (10881767001, Roche) or T3 RNA polymerase (11031171001, Roche). 3 μg of total RNA was heated to 90°C for 2 min, held on ice for 2 min, and incubated in RNA structure buffer (10 mM Tris-HCl pH 7.0, 100 mM KCl, and 10 mM $MgCl_2$) to allow the formation of the proper secondary structure. Cells at EB-D4 were lysed with RIP lysis buffer for 30 min on ice. IP was performed using streptavidin beads coated with biotin-labeled sense *Cpmer* or antisense *Cpmer*. The RNA-binding proteins were analyzed by LC-MS as described previously (Shevchenko et al., 2006). The mass spectrometry proteomics data have been deposited to the ProteomeXchange Consortium via the PRIDE (Perez-Riverol et al., 2022)partner repository with the dataset identifier PXD031814.

RIP assay

RIP was performed as previously described (Ng et al., 2012). Briefly, 5×10^6 cells were lysed with RIP buffer (100 mM KCl, 5 mM MgCl2, 10 mM HEPES pH 7.0, 0.5% NP-40, and 1 mM dithiothrectol) for 30 min on ice to facilitate lysis. Three micrograms of anti-Flag (GNI4110, GNI) antibody was used to bind *Cpmer* or its fragments after Flag-eEF1A2 was ectopically expressed in 293T cells. Coimmunoprecipitated RNAs were extracted and analyzed by qRT-PCR. The enrichment was calculated relative to the percentage of input.

MS2bp-YFP RNA pull-down

Briefly, cells were cotransfected with 4 μg of MS2bp-YFP overexpression plasmid, 4 μg of pMS2-*Cpmer* (or its fragments) or control vector with Renilla luciferase inserts (pMS2-Renilla) mixed with 24 μL Lipofectamine 3000 (Invitrogen). After 48 h, the cells were lysed with RIP buffer on ice for 30 min. The proteins were immunoprecipitated using control IgG (CST) or anti-GFP (ab290, Abcam). The RNA-protein complex was treated with RNAiso to purify RNA or SDS lysis buffer for western blotting.

Polysome profile analysis

Cells were treated with 100 μg/mL cycloheximide (CHX) (S7418, Selleck) and incubated for 10 min at 37°C before harvest. The cells were washed twice with ice-cold 1×PBS supplemented with 100 μg/mL CHX. After centrifugation for 5 min at 1000 rpm, the cells were lysed with 1 mL polysome extraction buffer (20 mM Tris-HCl pH 7.5, 100 mM KCl, 5 mM $MgCl_2$, and 0.5% NP-40) to which 100 μg/mL CHX, protease inhibitors, RNase inhibitor were added before use. The samples were incubated on ice for 10 min and centrifuged at 13,000 rpm for 10 min. The supernatant was loaded onto the top of a 10-50% sucrose gradient in a 13.2-mL tube (331372, Beckman Coulter) and centrifuged for 90 min in an SW41Ti swinging bucket rotor (3331336, Beckman Coulter) at 39,000 rpm at 4°C with maximum acceleration and braking. The gradient was pumped out and fractions were collected into 12 1.5-mL tubes, and RNA was extracted from each tube. The polysome profile was analyzed by qRT-PCR. Eomes and T mRNA distributions across the polysome profile are presented as percentages. For the analysis of co-sedimenting proteins, trichloro-acetic acid (TCA) was added to each fraction (final 10% v/v). Then proteins were precipitated overnight at 4°C and centrifuged at 13,000 rpm at 4°C for 20 min. Pellets were washed with ice cold acetone, then dissolved in 100 μL 2 × SDS loading buffer and heated at 95°C for 10 min.

RNA FISH

Cells were seeded on slides, washed once with 1×PBS, fixed with 4% paraformaldehyde at room temperature for 10 min, and then permeabilized with 0.2% Triton X-100 for 5 min. The cells were washed twice with 1×PBS and incubated with prehybridization buffer for 30 min at 37°C. The FISH

probe was added to the hybridization buffer at a dilution of 1:1000, and the cells were incubated in a humidified chamber in the dark at 37°C for 14 h. After hybridization, slides were washed 3 times with Wash Buffer I (4×SSC with 0.1% Tween-20), once each with Wash Buffer II (2×SSC) and Wash Buffer III (1×SSC) at 42°C for 5 min in the dark, and once with 1×PBS at room temperature. Then, the cells were stained with Hoechst 33342 for 10 min in the dark. Images were captured with a confocal microscope (Nikon). *Cpmer*-as-cy3 and *Cpmer*-s-cy3 probes were designed and synthesized by RiboBio Co., Ltd. Mouse U6 probes (LNC110103, RiboBio) and 18S probes (LNC110104, RibiBio) were used as the nuclear and cytoplasmic controls, respectively.

mRNA stability

Cells were treated with actinomycin D (S8964, Selleck) at a concentration of 100 μg/mL for different time intervals (0, 0.5, 1, 2, and 4 h). The cells were harvested, and RNA was extracted and analyzed by qRT-PCR. The remaining RNA levels of interest at each time point were normalized to those at the beginning.

Quantitative real-time PCR

Total RNA was extracted with RNAiso Reagent (TaKaRa) according to the manufacturer`s instructions. cDNA was synthesized with the PrimeScript RT reagent Kit (TaKaRa) by reverse transcribing 500 ng of total RNA. The resultant cDNA was diluted in double-distilled water, and 5 ng was used in each reaction. Quantitative real-time PCR was performed on an Mx3000 instrument (Agilent) using SYBR® Premix Ex Taq (TaKaRa, RR420A) and gene-specific primers. Samples were run in biological triplicate. Gene expression was normalized to the housekeeping gene GAPDH and calculated using the $2^{-\Delta\Delta Ct}$ method. Each experiment was performed in triplicate and repeated 3 times. The primer sequences are listed in Table S5.

Immunofluorescence staining

Cells were washed once with 1×PBS and fixed with 4% paraformaldehyde at room temperature for 20 min. Then, the cells were permeabilized with 0.2% Triton X-100 for 8 min. The cells were washed twice with 1×PBS, blocked in 10% FBS for 1 h, and incubated overnight with primary antibodies at the appropriate dilution at 4°C. Then, the cells were washed twice and incubated with AlexaFluor-488- or AlexaFluor-594-conjugated secondary antibody (Invitrogen) for 2 h at 4°C and counterstained with Hoechst 33342. Finally, the cells were examined under a fluorescence microscope to capture fluorescent images. Details of antibodies are listed in Table S6.

Western blotting

Cells were collected and washed in 1×PBS and incubated in 1×SDS lysis buffer supplemented with 1×Protease Inhibitor Cocktail (Roche) for 10 min on ice. The cells were centrifuged at 12,000 rpm for 15 min at 4°C, and equal amounts of cell lysates were resolved by 10% Bis-Tris SDS-PAGE and then transferred to polyvinylidene difluoride (PVDF) membranes (Millipore). Nonspecific binding was blocked by incubating in 3% BSA in TBST at 4°C for 2 h. Then, the blots were incubated with various primary antibodies in TBST at 4°C overnight. After washing with TBST 3 times, the blots were incubated with the appropriate secondary antibody for 2 h at 4°C. Signals were visualized by adding SuperSignal West Pico Chemiluminescent Substrate (Thermo Scientific) in enhanced chemiluminescence (ECL, ImageQuant LAS 4000 mini). GAPDH was used as the loading control. The anti-eEF1A antibody was unable to distinguish eEF1A1 and eEF1A2 protein. Details of antibodies are listed in Table S6.

References:

Ng, S.Y., Johnson, R., and Stanton, L.W. (2012). Human long non-coding RNAs promote pluripotency and neuronal differentiation by association with chromatin modifiers and transcription factors. EMBO J *31*, 522-533.

Perez-Riverol, Y., Bai, J., Bandla, C., Garcia-Seisdedos, D., Hewapathirana, S., Kamatchinathan, S., Kundu, D.J., Prakash, A., Frericks-Zipper, A., Eisenacher, M., et al. (2022). The PRIDE database resources in 2022: a hub for mass spectrometry-based proteomics evidences. Nucleic Acids Res *50*, D543-D552.

Shevchenko, A., Tomas, H., Havlis, J., Olsen, J.V., and Mann, M. (2006). In-gel digestion for mass spectrometric characterization of proteins and proteomes. Nat Protoc *1*, 2856-2860.

Table S4. Primers used for vector construction.			
Primer Name	**Sequence**		**Product Size**
Cpmer-KO-gRNA-1	CACCGAGCCTCTTGTGACTCGGGAC	S	N/A
	AAACGTCCCGAGTCACAAGAGGCTC	AS	
Cpmer-KO-gRNA-2	CACCGAGTGGGCCTGGTAGCTTACC	S	N/A
	AAACGGTAAGCTACCAGGCCCACTC	AS	
Rosa26-Cpmer-BglII	GGAAGATCTAGAGCCCTTTGTCGACTCTTT	F	586 bp
Rosa26-Cpmer-MfeI	CCGCAATTGCTTTTGTTTTTTGTTTCATGTG	R	
pBSK-Cpmer-EcoRI	CCGGAATTCAGAGCCCTTTGTCGACTCTTT	F	590 bp
pBSK-Cpmer-NotI	TTTATAGCGGCCGCTTTTGTTTTTTGTTTCATGT	R	
m-*Eef1a2*-sh1	CCGGGTCGGGTTCAATGTGAAGAATCTCGAGATTCTTCACATTGAACCCGACTTTTTG	S	N/A
	AATTCAAAAAGTCGGGTTCAATGTGAAGAATCTCGAGATTCTTCACATTGAACCCGAC	AS	
m-*Eef1a2*-sh2	CCGGGAGCGTAAGGAAGGAAATGCACTCGAGTGCATTTCCTTCCTTACGCTCTTTTTG	S	N/A
	AATTCAAAAAGAGCGTAAGGAAGGAAATGCACTCGAGTGCATTTCCTTCCTTACGCTC	AS	
Cpmer-sh1	CCGGGGATGATTCCAGACAGCAACCCTCGAGGGTTGCTGTCTGGAATCATCCTTTTTG	S	N/A
	AATTCAAAAAGGATGATTCCAGACAGCAACCCTCGAGGGTTGCTGTCTGGAATCATCC	AS	
Cpmer-sh2	CCGGGCAACCTCAAGGCTCTACATGCTCGAGCATGTAGAGCCTTGAGGTTGCTTTTTG	S	N/A
	AATTCAAAAAGCAACCTCAAGGCTCTACATGCTCGAGCATGTAGAGCCTTGAGGTTGC	AS	
h-CPMER-sh1	CCGGGTGATGTCTGCCACGAATATACTCGAGTATATTCGTGGCAGACATCACTTTTTG	S	N/A
	AATTCAAAAAGTGATGTCTGCCACGAATATACTCGAGTATATTCGTGGCAGACATCAC	AS	
h-CPMER-sh2	CCGGACCTGACCCCAGCGCTTAATTCTCGAGAATTAAGCGCTGGGGTCAGGTTTTTTG	S	N/A
	AATTCAAAAAACCTGACCCCAGCGCTTAATTCTCGAGAATTAAGCGCTGGGGTCAGGT	AS	
h-*EEF1A2*-sh1	CCGGGCTGGAAGGTGGAGCGTAAGGCTCGAGCCTTACGCTCCACCTTCCAGCTTTTTG	S	N/A
	AATTCAAAAAGCTGGAAGGTGGAGCGTAAGGCTCGAGCCTTACGCTCCACCTTCCAGC	AS	
h-*EEF1A2*-sh2	CCGGGCAGGACGTGTACAAGATTGGCTCGAGCCAATCTTGTACACGTCCTGCTTTTTG	S	N/A
	AATTCAAAAAGCAGGACGTGTACAAGATTGGCTCGAGCCAATCTTGTACACGTCCTGC	AS	

Fugw-Flag-*Eef1a2*-BamHI	CGCGGATCCATGGATTACAAGGATGACGACGATAAGGGCAAGGAGAAGACACACATCA	F	1434 bp
Fugw-*Eef1a2*-EcoRI	CCGGAATTCTCACTTGCCCGCTTTCTGAGCCTTCT	R	
Cpmer-AgeI	AAATATACCGGTAGAGCCCTTTGTCGACTC	F	588 bp
Cpmer-EcoRI	CCGGAATTCTTTTGTTTTTTGTTTCATGTG	R	
Cpmer-Exon2-AgeI	AAATATACCGGTGTCGAGGAGTCACCAGATGTGA	F	177 bp
Cpmer-Exon2-EcoRI	CCGGAATTCCTGTGGAGTAGGCTGACAAC	R	
Cpmer-Exon3-AgeI	AAATATACCGGTTGCTAGTGGGCCTGGTAGCT	F	316 bp (RP: Cpmer-EcoRI)
pMS2-Cpmer-HindIII-F	CCGGAAGCTTAGAGCCCTTTGTCGACTCTTTGGCT	F	587 bp
pMS2-Cpmer-EcoRI-R	CCGGGAATTCTTTTGTTTTTTGTTTCATGTGTGTGGCATG	R	
pMS2-*Renilla*-HindIII-F	CCGGAAGCTTATGACTTCGAAAGTTTATGATCCAG	F	956 bp
pMS2-*Renilla*-EcoRI-R	CCGGGAATTCTTATTGTTCATTTTTGAGAACTC	R	
Fugw-ms-*Eomes*-BamHI	GGCCGGATCCATGCAGTTGGGAGAGCAGCTCC	F	2267 bp
Fugw-ms-*Eomes*-EcoRI	CCGGGAATTCCTAGGGACTTGTGTAAAAAGCAT	R	
5` RACE primer	CAGTGGAAGATCAGTGAG	F	N/A
3` RACE primer	GGCTGAGATAACCAAGTC	R	
Fugw-Myc-Eomes-FL-5'	GGCCGGATCCATGGAGCAGAAACTCATCTCTGAAGAGGATCTGCAGTTGGGAGAGCAGCTCC	F	2118 bp
Fugw-Myc-Eomes-FL-3'	CCGGGAATTCCTAGGGACTTGTGTAAAAAGCAT	R	
Fugw-Myc-Eomes-⊿BS-R	CGGGGAGGAGGCTGACGCTCGAGTAGAAGTGCGCGCCGGG	R	125 bp (FP: Fugw-Myc-Eomes-FL-5')
Fugw-Myc-Eomes-⊿BS-F	CCGGCGCGCACTTCTACTCGAGCGTCAGCCTCCTCCCCGG	F	1974 bp (RP: Fugw-Myc-Eomes-FL-3')
Fugw-Myc-Eomes-⊿ELS-R	CTGCCCGGAAACTTCTTGGACCCTCCGCCTCCCCCTCCTCCTCCGCCTCCTCC	R	153 bp (FP: Fugw-Myc-Eomes-FL-5')
Fugw-Myc-Eomes-⊿ELS-F	GGAGGAGGAGGGGGAGGCGGAGGGTCCAAGAAGTTTCCGGGCAGTCTC	F	1938 bp (RP: Fugw-Myc-Eomes-FL-3')
Fugw-h-EOMES-BamHI	CCGGACCGGTATGCAGTTAGGGGAGCAGCTCT	F	2261 bp
Fugw-h-EOMES-EcoRI	CCGGGAATTCTTAGGGAGTTGTGTAAAAAGCATAA	R	
Fugw-Flag-h-*EEF1A2*-AgeI	CCGGACCGGTATGGATTACAAGGATGACGACGATAAGGGCAAGGAGAAGACCCAC	F	1436 bp
Fugw-h-*EEF1A2*-EcoRI	CCGGGAATTCTCACTTGCCCGCCTTCTGCG	R	
Abbreviation: RP: Reverse Primer; FP: Forward Primer			

Table S5. Primers used in RT-qPCR.				
Gene Name	**Forward Sequence**	**Reverse Sequence**	**Species**	**Product Size**
Gapdh	GTGTTCCTAACCCCAATGTGTC	ATTGTCATACCAGGAAATGAGCTT	mouse/ human	248 bp
Nkx2.5	ACATTTTACCCGGGAGCCTA	CGCTCCAGCTCGTAGACC	mouse	194 bp
cTnT	CGTGGAGAAGGACCTGAATG	CCCGCTCATTGCGAATAC	mouse	152 bp
Eomes	CCCTATGGCTCAAATTCCAC	CCAGAACCACTTCCACGAAA	mouse	141 bp
T	GCTCTAAGGAACCACCGGTCATC	ATGGGACTGCAGCATGGACAG	mouse	111 bp
Cpmer	GTCGAGGAGTCACCAGATGT	GGAGTAGGCTGACAACCATGA	mouse	152 bp
Eef1a2	ACTCCACGGAACCAGCCTA	GGGCAGGATTGTGTCCAGG	mouse	245 bp
Rpsa	TGCGGGAACCCACTTAGGT	AGGATTCTCGATGGCAACAATAG	mouse	154 bp
Rpl3	GGAAAGTGAAGAGCTTCCCTAAG	CTGTCAACTTCCCGGACGA	mouse	106 bp
Eef1a1	CAACATCGTCGTAATCGGACA	GTCTAAGACCCAGGCGTACTT	mouse	160 bp
Eif2s	CACCGCTGTTGACAGTCAGAG	GCAAACAATGTCCCATCCTTACT	mouse	142 bp
Tbx5	ATGGCCGATACAGATGAGGG	TTCGTGGAACTTCAGCCACAG	mouse	207 bp
Myh6	GACGCCCAGATGGCTGACTT	GGTCAGCATGGCCATGTCCT	mouse	276 bp
Tbx20	AAACCCCTGGAACAATTTGTGG	CATCTCTTCGCTGGGGATGAT	mouse	171 bp
Acta1	CCCAAAGCTAACCGGGAGAAG	CCAGAATCCAACACGATGCC	mouse	134 bp
Cpmer-E1	GCCCTTTGTCGACTCTTTGG	CCAACAGAGACTGACCCTCCT	mouse	103 bp
Cpmer-E3	AGCTCTGGGTTGGACTGAGA	TTTCATGTGTGTGGCATGTG	mouse	191 bp
Col1a1	GCTCCTCTTAGGGGCCACT	CCACGTCTCACCATTGGGG	mouse	103 bp
Col3a1	CTGTAACATGGAAACTGGGGAAA	CCATAGCTGAACTGAAAACCACC	mouse	144 bp
Ckap4	TCCCGTCAGAGGGATGAGC	GCTGGGAGTTTCTCAGGAGG	mouse	109 bp
CPMER	CCAAATGTGAAGGTGTAA	GCCAATCTTAATCTGACA	human	94 bp
CTNT	ACAGAGCGGAAAAGTGGGAAG	TCGTTGATCCTGTTTCGGAGA	human	230 bp
TBX20	TCGTCCCTGTGGACAACAAG	TTCAGGTTGAGCAATGAGGCT	human	286 bp
MYH6	CGGTGCTTTTCAACCTCAAGG	GGACTGGTTCTCCCGATCTGT	human	221 bp
ACTA1	GGCATTCACGAGACCACCTAC	CGACATGACGTTGTTGGCATAC	human	84 bp
EEF1A2	TCGTGGGCGTGAACAAAATG	GCTGACTTCCTTGACGATCTC	human	80 bp
EOMES	CTGCCCACTACAATGTGTTCG	GCGCCTTTGTTATTGGTGAGTTT	human	211 bp
T	TATGAGCCTCGAATCCACATAGT	CCTCGTTCTGATAAGCAGTCAC	human	109 bp

Table S6. Antibodies used in the study.						
Antibodies	**Company**	**Catalog**	**Species**	**Dilution WB**	**Dilution IF**	**Dilution FACS**
Anti-cTnT	Abcam	ab8295	Mouse	N/A	1:1000	N/A
Anti-Flk1	Miltenyi Biotec	130-102-559	Mouse	N/A	N/A	1:250
Anti-Pdgfrα	Miltenyi Biotec	130-109-784	Mouse	N/A	N/A	1:250
Anti-eEF1A	Santa Cruz	sc-377439	Mouse	1:500	N/A	N/A
Anti-GAPDH	Bioworld	AP0063	Rabbit	1:3000	N/A	N/A
Anti-EOMES	Abcam	ab23345	Rabbit	1:2000	1:1000	N/A
Anti-T	Abcam	ab209665	Rabbit	1:2000	1:1000	N/A
Anti-GFP	Abcam	ab290	Rabbit	N/A	1:1000	N/A
Anti-Myc tag	Abcam	ab9132	Mouse	1:3000	N/A	N/A
Anti-Sox2	CST	#23064	Rabbit	1:1000	N/A	N/A
Anti-Oct4	Abcam	ab19857	Rabbit	1:2000	N/A	N/A
Anti-Klf4	Santa Cruz	sc-20691	Rabbit	1:2000	N/A	N/A
Anti-mouse IgG, HRP	CST	7076s	N/A	1:3000	N/A	N/A
Anti-Rabbit IgG, HRP	CST	7074s	N/A	1:3000	N/A	N/A

Supplementary Data

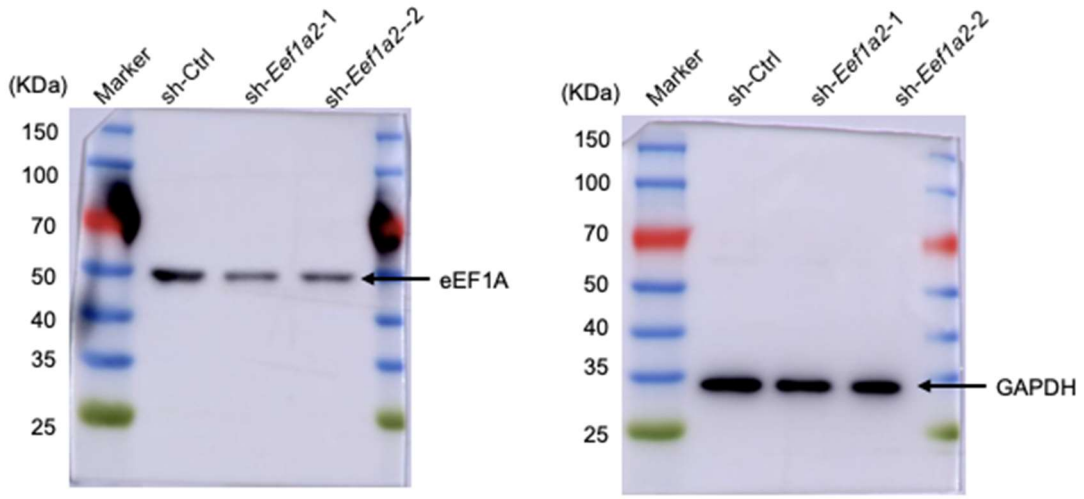

Whole membrane image 1. The efficiency of *Eef1a2* knockdown at mesoderm stage. Related to Figure 3F.

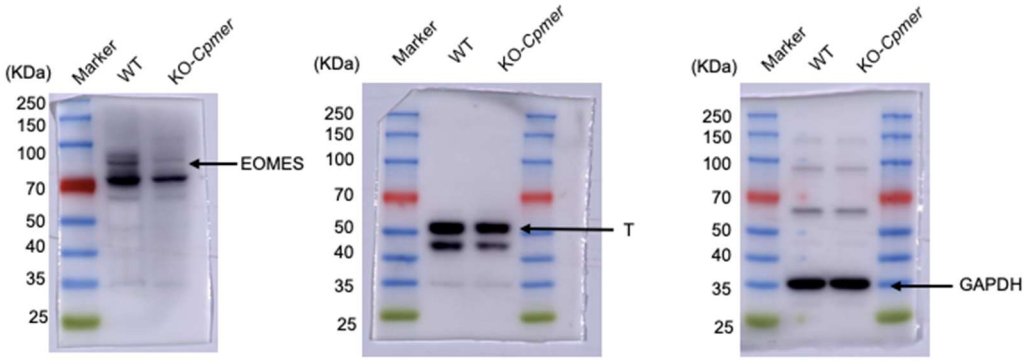

Whole membrane image 2. The EOMES and T protein levels at mesoderm stage in the WT and KO-*Cpmer* cells. Related to Figure 4B.

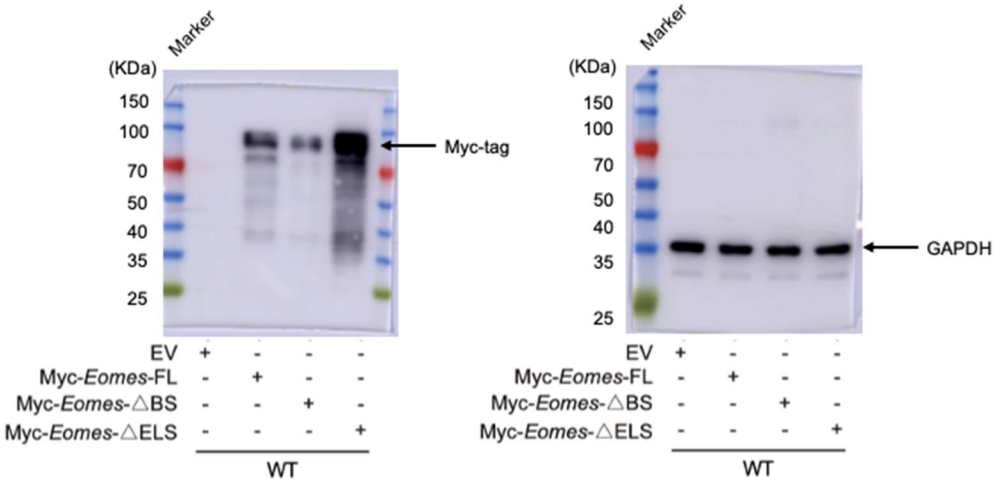

Whole membrane image 3. The exogenous Eomes expression in the WT cells transfected with full-length (FL) or deletion mutant *Eomes* at mesoderm stage. Related to Figure 4G.

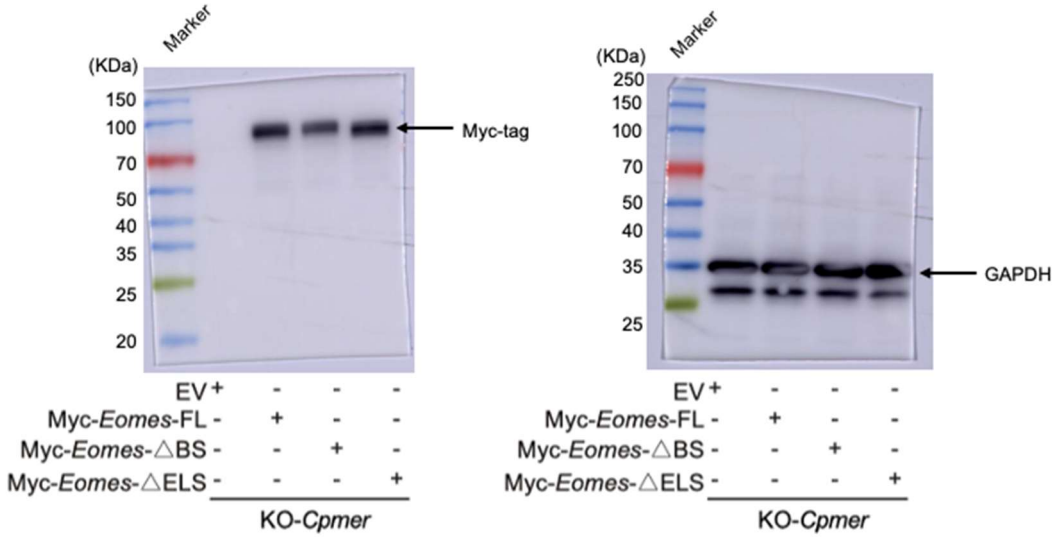

Whole membrane image 4. The exogenous Eomes expression in the KO-*Cpmer* cells transfected with FL or deletion mutant *Eomes* at mesoderm stage. Related to Figure 4H.

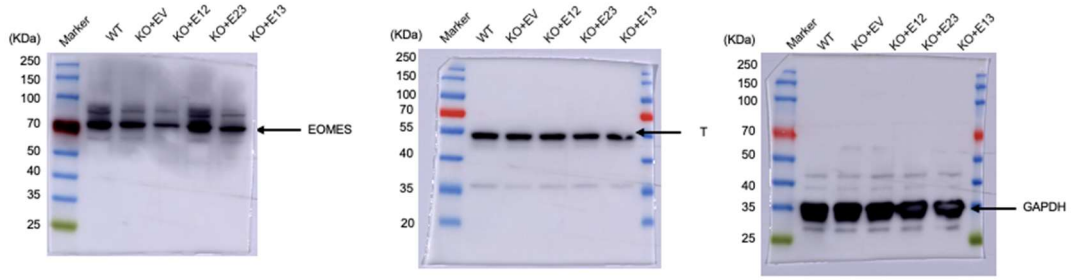

Whole membrane image 5. The EOMES and T protein levels in the WT and KO-Cpmer cells transfected with the double-exon mutants of *Cpmer* at mesoderm stage. Related to Figure 5E.

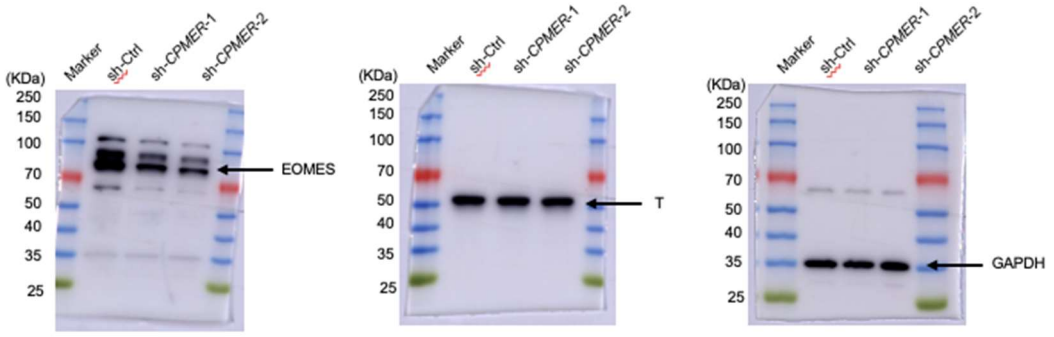

Whole membrane image 6. The EOMES and T protein levels in *CPMER*-knockdown cells at mesoderm stage. Related to Figure 6C.

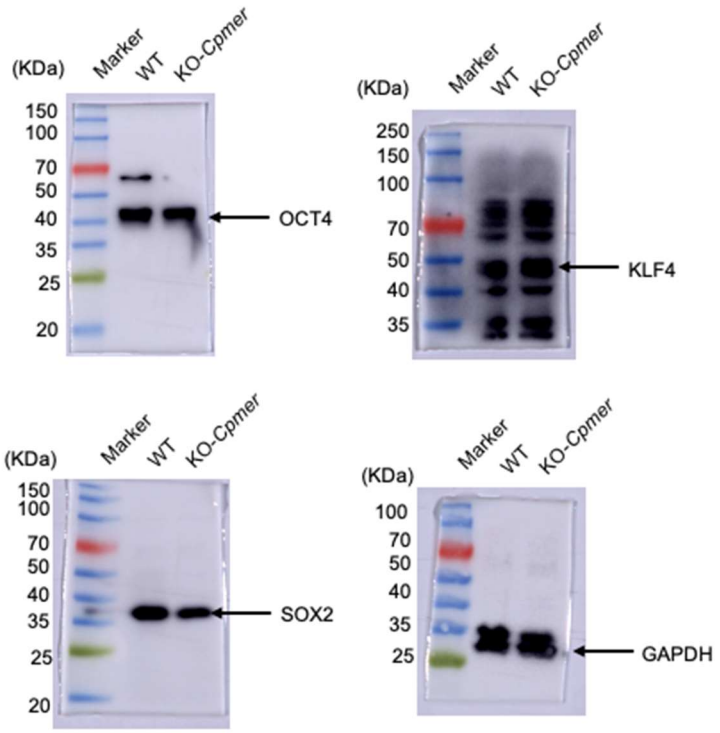

Whole membrane image 7. The expression level of pluripotency markers in the WT and KO-*Cpmer* cells. Related to Figure S2C.

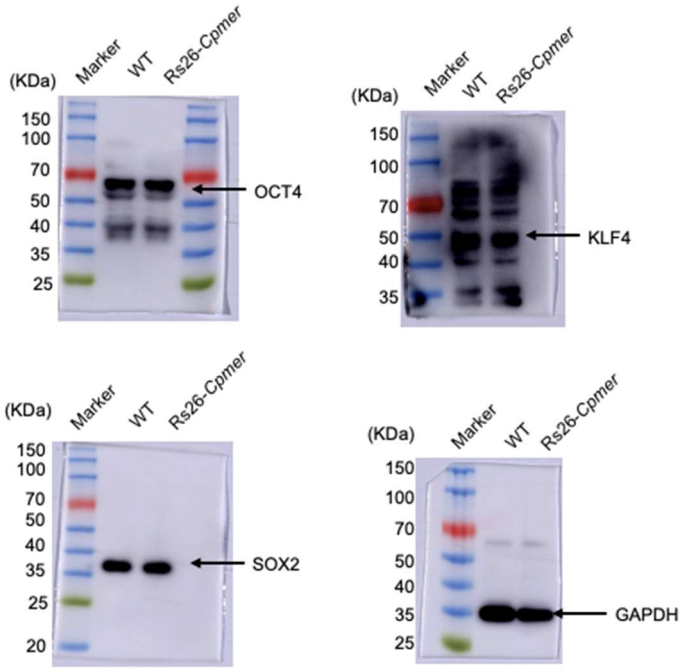

Whole membrane image 8. The expression level of pluripotency markers in the WT and Rs26-*Cpmer* cells. Related to Figure S2I.

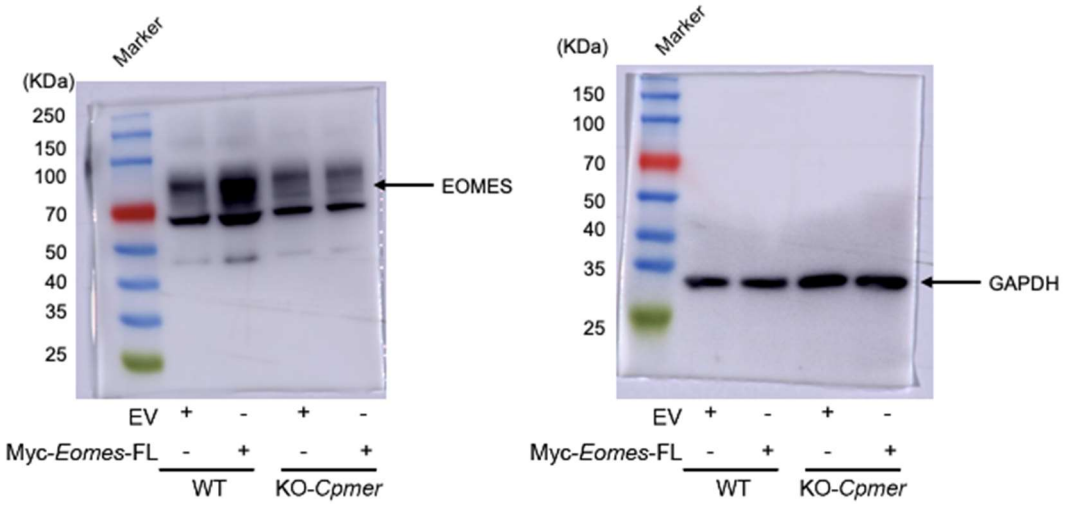

Whole membrane image 9. The EOMES levels in the WT and KO-Cpmer cells transfected with Myc-*Eomes*-FL at mesoderm stage. Related to Figure S4A.

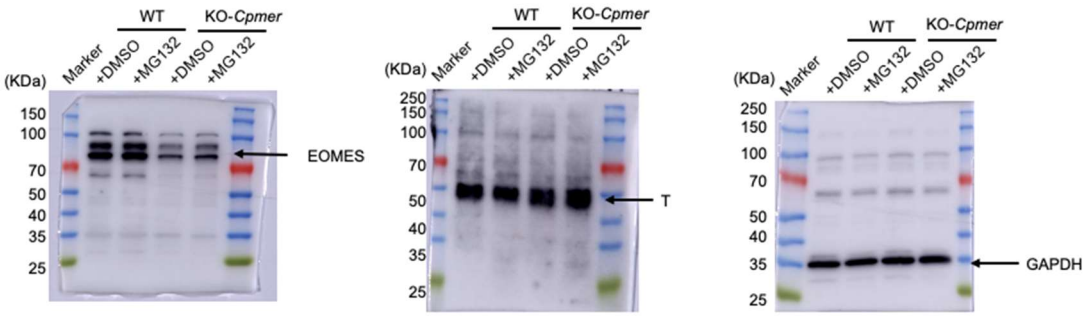

Whole membrane image 10. The EOMES and T levels in the WT and KO-*Cpmer* cells treated with MG132 at mesoderm stage. Related to Figure S4C.

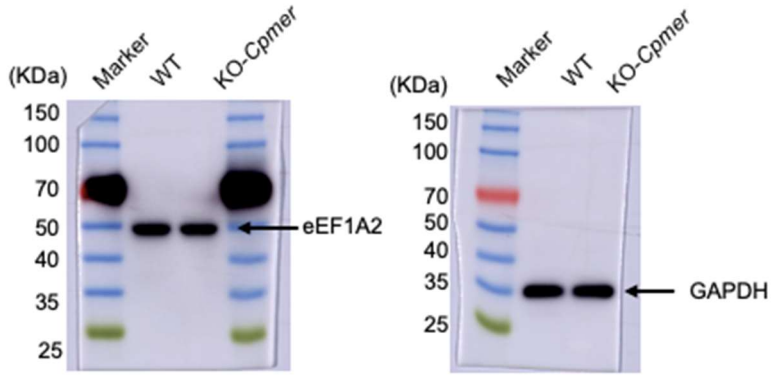

Whole membrane image 11. The eEF1A levels in the WT and KO-*Cpmer* cells. Related to Figure S4F.

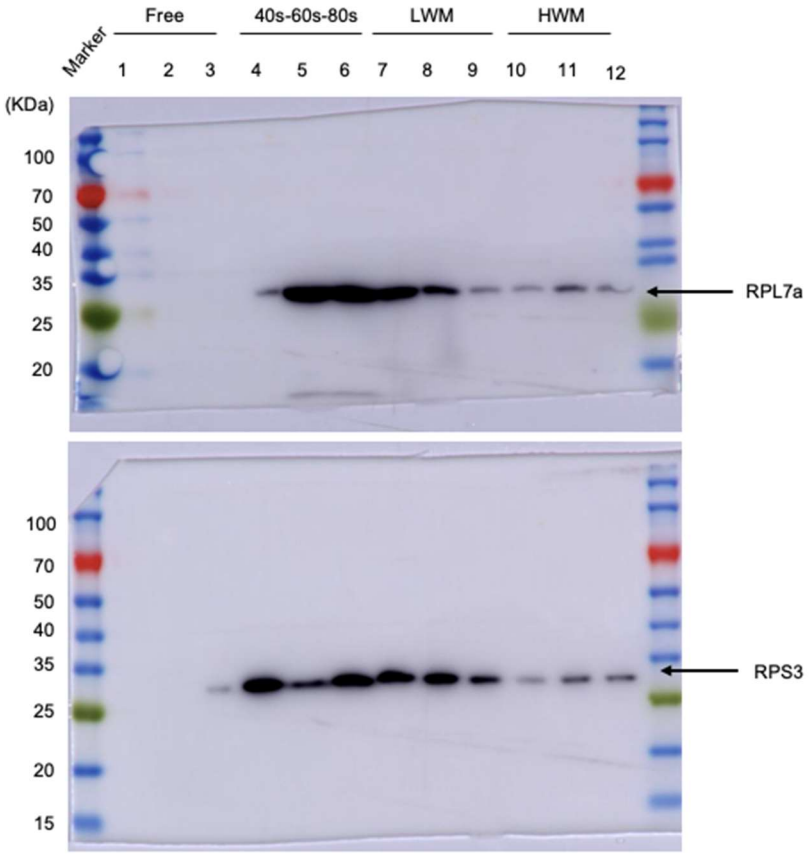

Whole membrane image 12. Western blotting analysis of polysome profile with RPL7a and RPS3 at mesoderm stage. Related to Figure S4G.

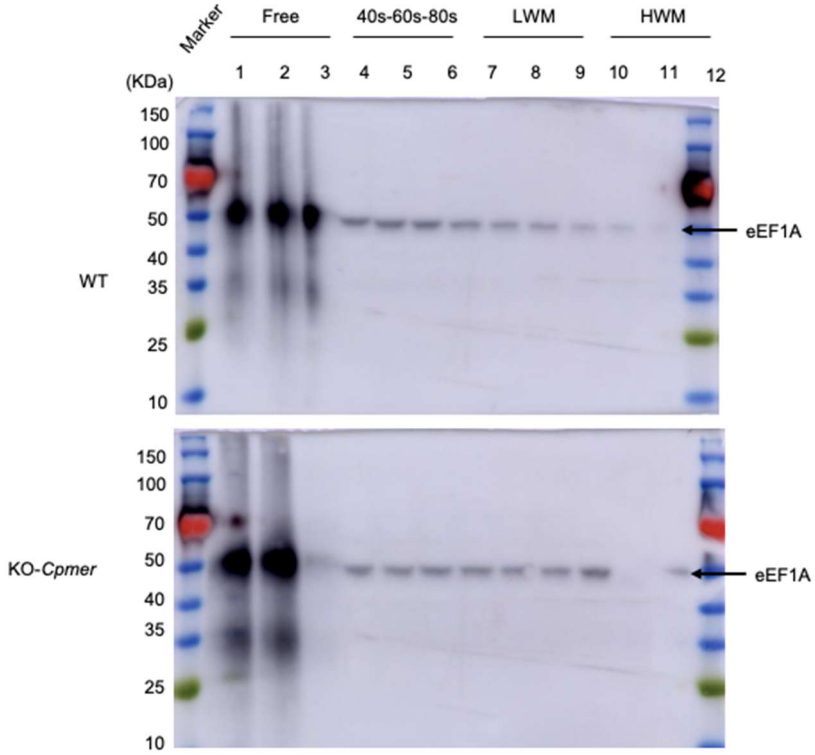

Whole membrane image 13. The eEF1A distribution in polysome fractions of the WT and KO-*Cpmer* cells at mesoderm stage. Related to Figure S4H.

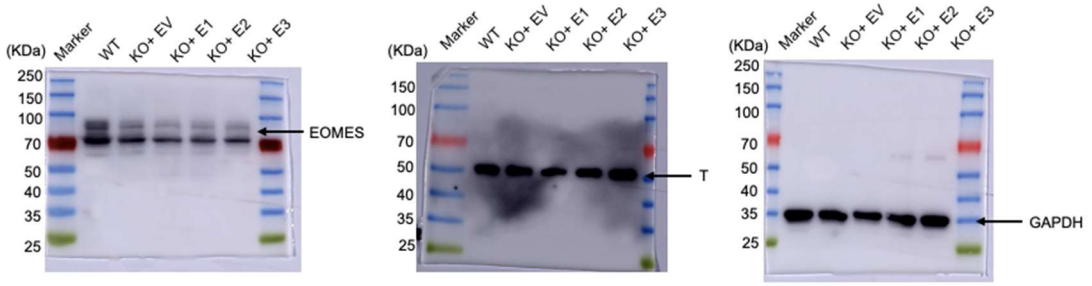

Whole membrane image 14. The EOMES and T expression levels in the KO-Cpmer cells transfected with different single-exon mutants of *Cpmer* at mesoderm stage. Related to Figure S5E.